

1 **Machine learning-constrained projection of bivariate hydrological**
2 **drought magnitudes and socioeconomic risks over China**

3 Rutong Liu¹, Jiabo Yin^{1*}, Louise Slater², Shengyu Kang¹, Yuanhang Yang¹, Pan Liu¹, Jiali Guo^{3,4},
4 Xihui Gu⁵, Xiang Zhang⁶, Aliaksandr Volchak⁷

5 ¹State Key Laboratory of Water Resources Engineering and Management, Wuhan University, Wuhan,
6 Hubei, 430072, P.R. China

7 ²School of Geography and the Environment, University of Oxford, Oxford, UK

8 ³Engineering Research Center of Eco-environment in Three Gorges Reservoir Region, Ministry of
9 Education, China Three Gorges University, Yichang, Hubei 443002, China

10 ⁴College of Hydraulic and Environmental Engineering, China Three Gorges University, Yichang,
11 Hubei 443002, China

12 ⁵School of Environmental Studies, China University of Geosciences, Wuhan 430074, China

13 ⁶National Engineering Research Center of Geographic Information System, School of Geography
14 and Information Engineering, China University of Geosciences, Wuhan 430074, China

15 ⁷Engineering Systems and Ecology Faculty, Brest State Technical University, Moskovskaya 267,
16 224017 Brest, Belarus

17

18

19 *Correspondence: Jiabo Yin (jboyn@whu.edu.cn)

20

21 **Abstract**

22 Climate change influences the water cycle and alters the spatiotemporal distribution of hydrological
23 variables, thus complicating the projection of future streamflow and hydrological droughts. Although
24 machine learning is increasingly employed for hydrological simulations, few studies have used it to project
25 hydrological droughts, not to mention the bivariate risks, referring to drought duration and severity, as well
26 as their socioeconomic effects under climate change. We developed a cascade modeling chain to project
27 future bivariate hydrological drought characteristics in 179 catchments over China, using 5 bias-corrected
28 GCM outputs under three shared socioeconomic pathways, five hydrological models and a deep learning
29 model. We quantified the contribution of various meteorological variables to daily streamflow by using a
30 random forest model, then employ terrestrial water storage anomalies and a standardized runoff index to
31 evaluate recent changes in hydrologic drought. Subsequently, we constructed a bivariate framework to jointly
32 model drought duration and severity by using Copula functions and the most likely realization method.
33 Finally, we used this framework to project future risks of hydrological droughts as well as associated exposure
34 of gross domestic product and population. Results showed that our hybrid hydrological-deep learning model
35 achieved >0.8 Kling-Gupta efficiency in 161 out of 179 catchments. By the late 21st century, bivariate drought
36 risk is projected to double over 60% of catchments mainly located in Southwest China under SSP5-85, which
37 shows the increase of drought duration and severity. Our hybrid model also projected substantial GDP and
38 population exposures by increasing bivariate drought risks, suggesting an urgent need to design climate
39 mitigation strategies toward a sustainable development pathway.

40 **1 Introduction**

41 In a warming world, the change of the global water cycle is expected to alter the regional and seasonal
42 distribution of key hydrological variables such as precipitation and evapotranspiration (Allan et al., 2020;
43 Yin et al., 2023b). As precipitation patterns are particularly sensitive to changes in atmospheric forcing and
44 local conditions, precipitation extremes are generally increasing globally, exacerbating spatial heterogeneity
45 of precipitation (Donat et al., 2016; Tabari, 2020). A suite of Shared Socioeconomic Pathways (SSPs) has
46 been proposed to simulate different possible future scenarios of social responses to climate change, and these
47 are employed to investigate the possible effects of long-term climate change (Meinshausen et al., 2020; Zhang
48 et al., 2021). By using the SSP framework, numerous works have indicated that the redistribution of
49 precipitation may lead to the decline of water storage in some regions, and intensify water scarcity in arid
50 regions (Sönmez and Kale, 2018; Woolway et al., 2020; Yao et al., 2023). Under increasing atmospheric
51 greenhouse gases, numerous studies have reported a widespread increase in drought events, even in areas
52 with increasing annual runoff (Dai et al., 2018). The rapidly changing distribution of precipitation and other
53 meteorological elements under climate change complicates projection of future runoff and drought.

54 China's socioeconomic development, particularly its agricultural sector, is threatened by the rapid
55 intensification of extreme hazards under climate change (Piao et al., 2010). Over the past years, China has
56 been hit by severe drought events which have caused considerable damage to ecosystem productivity and
57 socio-economic growth (Yin et al., 2023; Zhai and Zou, 2005). For instance, one extreme drought in Sichuan
58 Province in 2022 resulted in power shortages and led to economic losses of 669 million dollars. Water
59 shortage is also a key challenge that hinders the sustainable development of the North China Plain (Chen and
60 Yang, 2013). Over the period of 1985-2014, drought accounted for about 19% of economic losses among all
61 meteorological hazards (Chen and Sun, 2019). With continuing global warming, the economic losses from
62 severe drought events might increase by over ten billion US dollars per year by the late 21st century,
63 underscoring the importance of projecting future droughts over China (Lu et al., 2023).

64 Droughts can be triggered by divergent mechanisms, and are thus distinguished according to the type of
65 drought, such as meteorological and hydrological drought (Yihdego et al., 2019). The majority of studies
66 have focused on meteorological droughts, which can then be translated to a hydrological drought, while fewer
67 works have focused on hydrological drought probably due to a lack of measurements like the standardized
68 runoff index (SRI) (Barker et al., 2016; Kumar et al., 2016; Tirivarombo et al., 2018). Furthermore,
69 hydrological droughts are not only affected by the water cycle but also by human interventions, which makes
70 them difficult to accurately be predicted (Wu et al., 2021). Currently, the majority of drought impact
71 assessments focus on the investigation of individual drought variables (i.e., drought duration, severity,
72 intensity, etc.) through univariate probabilistic models and stochastic theory (Byakatonda et al., 2018;
73 Myronidis et al., 2018; Zhang et al., 2022). However, univariate drought analysis cannot accurately describe
74 the probability of drought events, because droughts of either long duration or severe intensity can lead to

75 substantial socio-ecosystem damages (Castle et al., 2014; Udall and Overpeck, 2017). Therefore, the bivariate
76 framework based on Copula functions has been developed for drought projection, compensating for the
77 incompleteness of a single variable analysis (Ayantobo et al., 2017; Nabaei et al., 2019). At present, studies
78 on hydrological drought within a bivariate framework are still lacking. Beyond the choice of approach
79 (univariate or bivariate), the Gravity Recovery and Climate Experiment (GRACE) and GRACE-FO (GRACE
80 Follow-On) satellites now provide two decades of large-scale terrestrial water storage (TWS) data, which
81 captures the water deficit in various forms on land and can be used to monitor droughts (Schmidt et al., 2006).
82 The drought severity index based on TWS (TWS-DSI) can be used to monitor past drought events, which
83 also shows potential advantages in drought warning, forecasting, and projection (Nie et al., 2018; Pokhrel et
84 al., 2021).

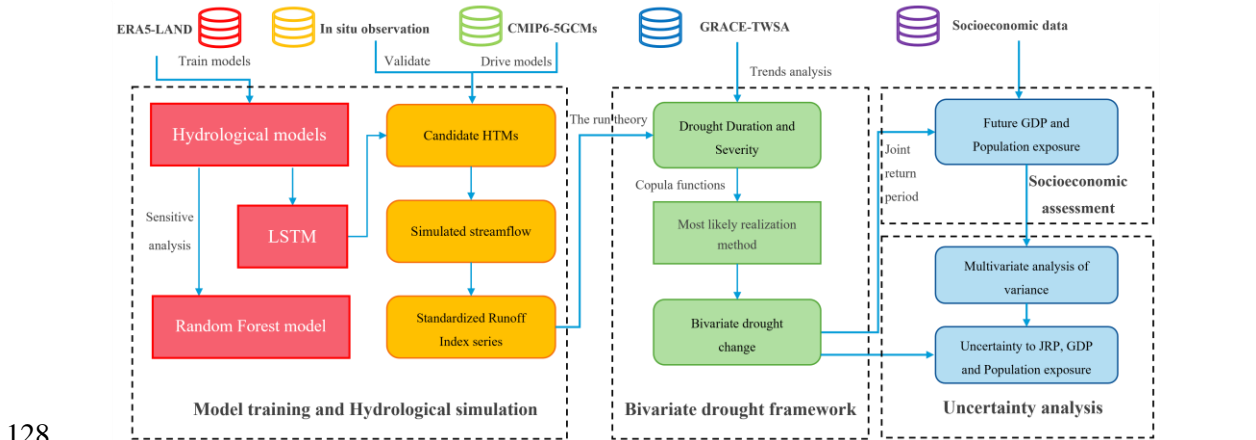
85 In recent decades, many studies have used bias-corrected outputs from Global Climate Models (GCMs)
86 to project future hydrological drought scenarios (e.g., (Ashrafi et al., 2020; Dixit et al., 2022; Kim et al.,
87 2021). The growing application of machine learning has revealed a high potential for improving the accuracy
88 of hydrological simulation and prediction (Mokhtar et al., 2021). In recent years, many machine learning
89 algorithms have been adopted in drought simulation and produce good performance, such as wavelet neural
90 networks (WNNs) (Xiuji et al., 2022), support vector machines (SVMs) (Zhu et al., 2021) and long short-
91 term memory neural networks (LSTMs) (Dikshit et al., 2021a)). These algorithms can be used to simulate
92 the evolution of future droughts and construct risk maps for drought contingency planning (Rahmati et al.,
93 2020). Among the different models, the LSTMs can effectively simulate short-term and long-term streamflow
94 series, and their performances have been validated at short temporal scales (Dikshit et al., 2021b; Kang et al.,
95 2023).

96 In this study, we projected changes in bivariate hydrological drought characteristics (duration and
97 severity) and their associated socioeconomic risks under three SSPs (i.e., SSP1-26, SSP3-70, and SSP5-85)
98 over 179 catchments in China. To achieve this, we combined five hydrological models and a deep learning
99 model (i.e., the LSTM), and then drove the hybrid models with the five bias-corrected GCMs outputs under
100 the Coupled Model Intercomparison Project phase six (CMIP6). Then, we employed a machine learning-
101 based framework (i.e., Random Forest, RF model) to quantify the sensitivity of daily streamflow to different
102 meteorological variables. We employed the run theory and two drought metrics, the SRI and TWS-DSI, to
103 identify and explore recent changes in drought characteristics. In addition, we used Copula functions to build
104 the bivariate model of drought duration and severity during both reference and future periods. After
105 identifying shifts in bivariate drought characteristics based on the most likely realization approach, we
106 projected the exposure of gross domestic product (GDP) and population to increasing drought risks in the
107 future. Finally, we decomposed the uncertainties arising from different sources by employing the multivariate
108 analysis of variance (MANOVA) method. This study illustrated the used materials and methods in Section 2
109 and Section 3, respectively. We compared SRI and TWS-DSI in assessing drought conditions in Section 4.1.
110 The contribution of meteorological factors to simulate streamflow and the calibration of hybrid terrestrial
111 models were shown in Section 4.2. The evolution of univariate droughts was projected in Section 4.3. The

112 bivariate droughts of future scenarios and associated socioeconomic exposures were evaluated in Section 4.4.
 113 We discussed the uncertainty of our analysis and main limitations of this study in Section 5, and finally
 114 summarized our work in Section 6.

115 **2. Methodology**

116 The workflow of this study is divided into four modules (Figure 1), described briefly below and detailed
 117 in the following sections. In step 1, the hydrological models and LSTM are trained using the ERA5-Land
 118 dataset, and then the output of HMs is used as input to feed the LSTM, thus we build the hybrid terrestrial
 119 models (HTMs). In step 2, the trained HTMs are validated using in situ streamflow observations, then driven
 120 by using the outputs of five GCMs from the CMIP6 to project streamflow and the SRI series. In step 3,
 121 monthly drought characteristics (i.e., drought duration and severity) are defined using run theory and
 122 combined with Copula functions to construct a bivariate drought framework. Future bivariate drought change
 123 is evaluated using the most likely realization method. Meanwhile, the TWS measurements from GRACE
 124 missions are also employed to characterize recent changes in TWS-based droughts, which are also compared
 125 with the hydrological droughts. In step 4, we employ future scenarios of GDP and population alongside our
 126 future drought projections to produce a socioeconomic assessment of drought exposure over China. Finally,
 127 we examine the contribution of uncertainty from different sources in projecting drought change and exposure.



129 **Figure 1. Schematic flowchart of the method, including ML-constrained hydrological simulations, evaluation of**
 130 **bivariate hydrologic drought characteristics and change, and the socioeconomic evaluation to drought exposure**
 131 **under climate change.**

132 **2.1 Derivation of 2-meter relative and specific humidity**

133 As relative humidity and specific humidity are not directly available from the ERA5-land dataset, we
 134 estimate these two variables based on the physical relationship in atmosphere. The Clausius–Clapeyron
 135 relationship is used to derive saturated vapor pressure (e_s) and air temperature (T), and is expressed as follows
 136 (Koutsoyiannis, 2012):

137
$$e_s(T) = e_0 \exp \left[\left(\frac{1}{T_0} - \frac{1}{T} \right) \frac{L_0}{R_0} \right] \quad (1)$$

138 where T_0 , e_0 , L_0 and R_0 are freezing temperature in Kalvin, saturated vapor pressure under freezing
 139 temperature, latent heat of vaporization and gas constant of water vapor, with a value of 273.15 K, 611 Pa,
 140 $2.5 \times 10^6 \text{ J kg}^{-1}$, $461 \text{ J kg}^{-1} \text{ K}^{-1}$, respectively;

141 Since near-surface relative humidity (RH) can't be directly obtained from the ERA5-Land dataset, the
 142 2m temperature (T_{2m}) and dew-point temperature (T_d) are substituted into equation (1) to calculate RH :

143
$$RH = \frac{e_s(T_d)}{e_s(T_{2m})} = \exp \left[\left(\frac{1}{T_{2m}} - \frac{1}{T_d} \right) \frac{L_0}{R_0} \right] \quad (2)$$

144 Then, the near-surface air pressure (ps) and T_d are used to deduce the specific humidity (SH), which is
 145 mathematically expressed as follows (Simmons et al., 1999):

146
$$SH = \frac{0.622 \times e_s(T_d)}{ps - 0.378 e_s(T_d)} \quad (3)$$

147 2.2 Sensitivity analysis on meteorological variables for runoff

148 The RF model (Catani et al., 2013) is used to calculate the sensitivity of runoff to different
 149 meteorological variables, including precipitation (pr), air pressure (ps), surface downwelling shortwave and
 150 longwave radiation ($srsds$ and $srlsds$), RH , SH , average temperature, maximum and minimum temperature.
 151 The contribution of a key variable is derived by using the pre-established model, the perturbed meteorological
 152 variable and remaining (non-perturbed) variables (Antoniadis et al., 2021; Green et al., 2020). The percentage
 153 change in streamflow is derived from the following equation:

154
$$S_i = \frac{\text{mean}(R_{(i+1SD)} - R_{(all)})}{\text{stdev}(R_{obs})} \times 100\% \quad (4)$$

155 where S_i indicates the sensitivity of streamflow to i^{th} meteorological variable, which are pr , ps , SH , RH , $srlsds$,
 156 $srsds$ and temperature; R_{obs} is the observation of streamflow which has units of m^3/s ; $R_{(i+1SD)}$ is the simulated
 157 streamflow by perturbing i by +1 SD; $R_{(all)}$ is the streamflow simulated by all meteorological variables; stdev
 158 (R_{obs}) represents the standard deviation of R_{obs} .

159 2.3 Deep learning-constrained hydrological modeling

160 2.3.1 Conceptual hydrological models

161 For preliminary hydrological simulations, we select five hydrological models to represent hydrological
 162 characteristics under different environments. The GR4J (Génie Rural à 4 paramètres Journalier) is a lumped
 163 model with 4 parameters developed by Perrin et al. (2003). GR4J consists of two water store modules (runoff

164 yielding and routing) and uses daily rainfall and evapotranspiration as inputs to simulate streamflow series
165 (Kunnath-Poovakka and Eldho, 2019). This model has been successfully used to simulate hybrid runoff
166 processes on many continents (Gu et al., 2023; Shin and Kim, 2021). Additionally, we use the temperature-
167 based method (Oudin et al., 2005) to estimate the potential evapotranspiration of the GR4J model.

168 The HBV (Hydrologiska Byråns Vattenbalansavdelning) model was initially developed by the Swedish
169 Meteorological and Hydrological Institute for Hydrological Forecasting (BERGSTRÖM and FORSMAN,
170 1973). This model includes five modules and one transform function to quantify hydrological variables (i.e.,
171 precipitation, snow, soil moisture, runoff, baseflow) (Bergström, 1995). It has been widely employed to
172 simulate streamflow, and it particularly has a good capacity for simulating snowmelt runoff (Kriauciuniene
173 et al., 2013).

174 The HMETs (hydrological model of École de technologie supérieure) model contains 21 parameters
175 and two reservoirs (i.e., the saturated and vadose zones), which is considered to efficiently complete
176 hydrological simulation in limited scales (Martel et al., 2017). The model can simulate six processes in water
177 cycle, including the accumulation, melts and refreezing of snow, water infiltration and routing, and
178 evapotranspiration (Qi et al., 2020). It has been growly used for streamflow simulation under climate change
179 and has shown great performance (Chen et al., 2018).

180 The SIMHYD (simple lumped conceptual daily rainfall-runoff) model is a daily rainfall-runoff model
181 developed by Porter and McMahon (1975). There are four types of water fluxes from different sources:
182 impervious areas, infiltration, interflow, and groundwater storage (Chiew et al., 2002). Although the model
183 was developed earlier, it has shown good accuracy in simulating runoff over China (Yu and Zhu, 2015).

184 The XAJ (Xinanjiang) model is a hydrological model, which can usually achieve better performance in
185 humid and semi-humid areas than in arid areas (Ren-Jun, 1992). As the model was developed based on the
186 underlying surface of the Yangtze River Basin in China, it is composed of a three-layer evapotranspiration
187 module with four parameters and separates the runoff into four components (i.e., surface water, groundwater,
188 interflow water and flow routing) (Tian et al., 2013). To date, it is widely reported that the XAJ model usually
189 shows a great performance in simulating hydrological conditions in China (Hu et al., 2005; Jiang et al., 2007).
190 However, due to inadequacies in the simulation of arid regions, the results of the XAJ model did not be
191 considered as the best option in northern China.

192 We used the SCE-UA (Shuffled Complex Evolution) approach to maximize the objective function (i.e.,
193 Kling-Gupta efficiency) to optimize these models (Duan et al., 1992). The most complete 20-year observation
194 period is selected to calibrate five models in each watershed by a daily time step. To calibrate the hydrological
195 models, a cross-validation method developed by Arsenault et al. (2017) is used for calibration, which employs
196 the odd years of data to calibrate models, and the even years of data to validate. As catchments are located in
197 different climatic regions, the parameters of models are calibrated for each catchment, which means that the
198 parameters are not universal. Although uncertainties shown by hydrological models are ineradicable, the
199 overall uncertainty is acceptable in the current scale after optimizing five hydrological models for each
200 catchment.

201 2.3.2 Hybrid scheme of hydrological model and machine learning

202 Recurrent neural network (RNN) models have had considerable success in hydrological modeling (Cho
203 et al., 2014; Sherstinsky, 2020). However, when considering long input sequences, RNNs struggle to capture
204 the relationships between distant points due to a phenomenon known as “long-term dependencies” (Yu et al.,
205 2019). With the development of deep learning, this problem can be successfully avoided by using LSTMs.

206 An LSTM cell includes input, output and forget gates. The input gate determines which new information
207 can be stored in the cell state, and the forget gate identifies which information will be discarded from the cell
208 state. The output gate controls what part of the cell state is selected as the output. The updated cell state is a
209 combination of the information retained and the new information to be added. By using this architecture, the
210 LSTM can avoid the problem of gradient vanishing or explosion during backpropagation, especially when a
211 series is long (Gers et al., 2000). The LSTM can be expressed as follows:

$$212 \quad fg_t = \sigma(W_{hf}hs_{t-1} + W_{xf}x_t + b_f) \quad (5)$$

$$213 \quad ig_t = \sigma(W_{hi}hs_{t-1} + W_{xi}x_t + b_{fg}) \quad (6)$$

$$214 \quad \tilde{c}_t = \tanh(W_{hc}hs_{t-1} + W_{xc}x_t + b_c) \quad (7)$$

$$215 \quad c_t = fg_t \cdot c_{t-1} + ig_t \cdot \tilde{c}_t \quad (8)$$

$$216 \quad og_t = \sigma(W_{ho}hs_{t-1} + W_{xo}x_t + b_o) \quad (9)$$

$$217 \quad hs_t = og_t \odot \tanh(c_t) \quad (10)$$

218 where x_t , fg_t , ig_t and og_t are input variables, and forget, input and output gates at time t , respectively; W
219 are the weights, where W_i , W_c , W_f and W_o are the weights of each gate, W_x are the weights of each gate at
220 time t , W_h are the weights of each gate at the former time $t - 1$; the operator ‘ \odot ’ is the symbol for the dot
221 product of two vectors; c_t and hs_t are the cell state of the LSTM and the hidden unit at time t , respectively;
222 c_{t-1} and hs_{t-1} at the former time $t - 1$; \tilde{c}_t is the activation function of hidden layer; b_i , b_f , b_o and b_c are
223 bias items and the; $\sigma(\cdot)$ and $\tanh(\cdot)$ are the sigmoid function and the hyperbolic tangent function,
224 respectively; at the initial moment, cell and hidden states are set to zero arrays.

225 The hydrological outputs together with other climate variables are used as inputs to feed the LSTM
226 model (i.e., the LSTM is thus constrained by the HMs). Because changes in meteorological variables require
227 some time to converge before they are reflected in the runoff, it is essential to calculate the lag time caused
228 by the flow convergence for the model. The catchment response lag time d is defined as the time during
229 which precipitation accumulates in the river to generate runoff for the gauge downstream, and is
230 mathematically expressed as follows (Berne et al., 2004; Ganguli and Merz, 2019):

231
$$d = 2.51A_d^{0.4} [\text{ hrs }] = 0.11A_d^{0.4} [\text{ days }] \quad (11)$$

232 where A_d (km²) represents the catchment area; meteorological variables from day $T-d$ to day T are employed
233 to drive HTMs.

234 We combine the five hydrological models with LSTM to construct five HTMs. To compare the
235 performance of the HTMs, we use ten HTMs as candidates for streamflow simulation in each catchment. The
236 calibrated HTMs are then driven by the outputs of five GCMs under each SSP (aggregated to produce a basin
237 average series) during 1985-2100 over 179 catchments to project future daily streamflow.

238 2.4 Drought indexes and run theory

239 The TWS-DSI is employed to measure the degree of terrestrial drought severity (Zhao et al., 2017). It
240 is a dimensionless standardized water storage anomaly index, which can indicate terrestrial drought
241 conditions when below the mean standard value. The TWS-DSI can be mathematically expressed as follows:

242
$$TWS-DSI_{x,y} = (TWS_{x,y} - \overline{TWS_y}) / \sigma_y \quad (12)$$

243 where $TWS_{x,y}$ is the TWS at year x and month y ; $\overline{TWS_y}$ and σ_y represent the means and standard deviation
244 of TWS at month y , respectively.

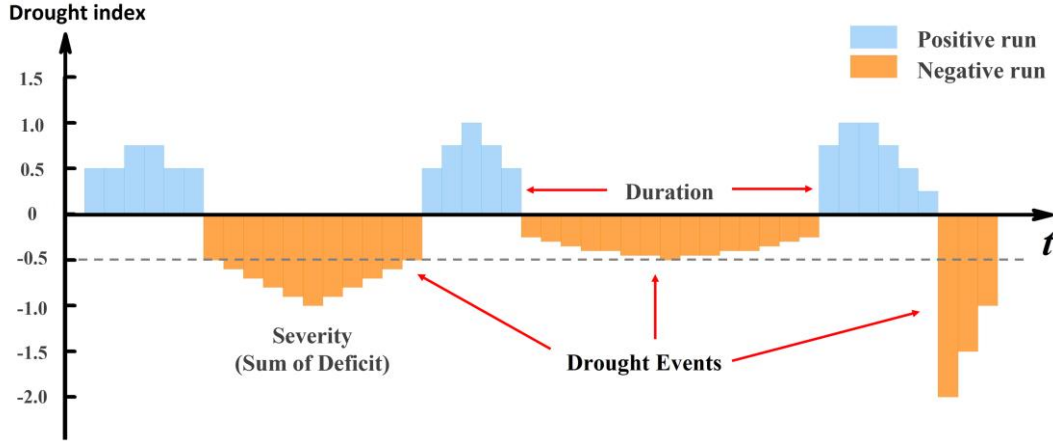
245 The SRI is a measure of the variability of runoff for a given duration based on the percentage of
246 accumulated runoff. (Shukla and Wood, 2008). The hydrological drought classification and ranges indicated
247 by SRI are shown in Table S1. To calculate the SRI, we simulate the retrospective time series of streamflow
248 and fit the sample series to a probability distribution. The SRI is considered to follow a Pearson type-III
249 distribution (Vicente-Serrano et al., 2012), and is calculated as follows:

250
$$SRI = \begin{cases} -\left(r - \frac{c_0 + c_1r + c_2r^2}{1 + d_1r + d_2r^2 + d_3r^3}\right) & 0 < F(x) \leq 0.5 \\ r - \frac{c_0 + c_1r + c_2r^2}{1 + d_1r + d_2r^2 + d_3r^3} & 0.5 < F(x) \leq 1 \end{cases} \quad (13)$$

251 where $r = \sqrt{\ln \left[\frac{1}{F(x)^2} \right]}$; $F(x)$ is the cumulative probability density of SRI; c_0 , c_1 , c_2 , d_1 , d_2 and d_3 are

252 the empirical constants, taken as 2.516, 0.803, 0.010, 1.433, 0.189, 0.001, separately.

253 After calculating the two drought indexes, the degree of water deficit can be determined according to
254 the Grades of Meteorological Drought and the previous classification (Dikici, 2020). Table S1 presents the
255 drought classification and thresholds used for identifying drought degrees. The run theory is employed to
256 obtain characteristics of drought events from the time series (Yevjevich, 1967). When the drought index is
257 below the mild drought (i.e., ≤ -0.5 drought index), a drought event is detected (Figure 2), and then the drought
258 duration and drought severity are extracted.



259

260 **Figure 2. Drought duration and severity identification based on run theory, where -0.5 denotes the drought**
 261 **threshold (grey dash line).**

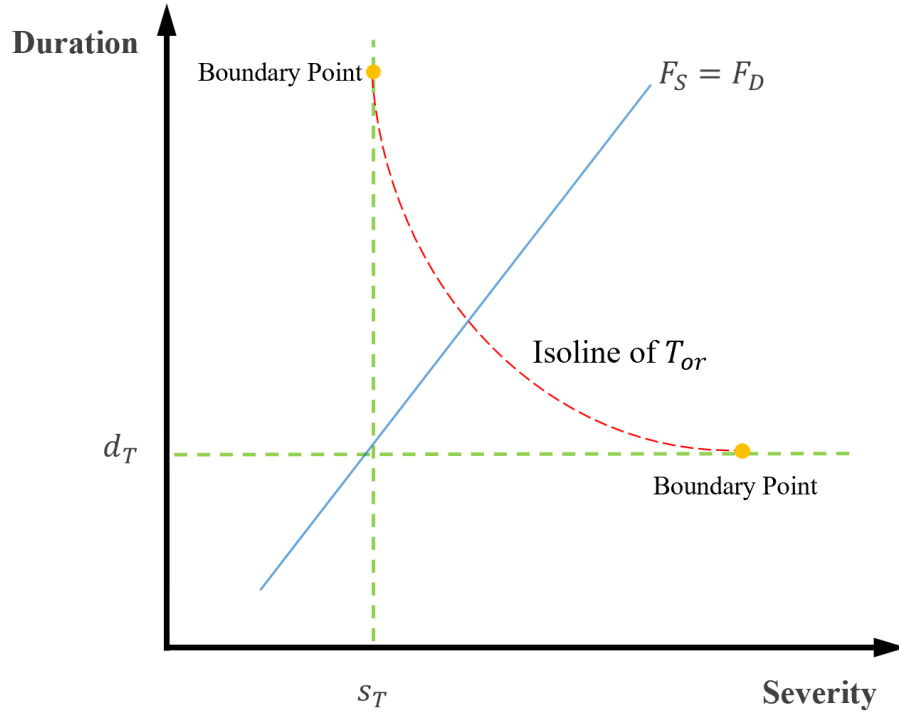
262 **2.5 Socioeconomic exposure assessments based on the Copulas and most likely realization**

263 To integrate the assessment of drought change arising from the duration and severity under climate
 264 change, we employed a Copula framework by constructing joint probability distribution of two variables.
 265 After extracting the drought duration (D) and severity (S), we fit their marginal distributions with seven
 266 distributions shown in Table S2. The OR case (i.e., a bivariate drought event is identified with either a high
 267 severity or long duration) of the joint return period (JRP) under a Copula-based framework is used to quantify
 268 the occurrence of drought events (Yin et al., 2020). The joint distribution of drought duration and severity is
 269 constructed by using a Copula function, which is valuable for describing correlated hydrological variables
 270 (Li, 1999). Unlike univariate drought frequency analysis, the JRP within a bivariate framework can be
 271 represented by an isoline, which contains infinite combinations of values of these two multivariate arrays of
 272 variables. It is important for risk assessments to select a representative combination along the isoline.
 273 Previous studies have only selected joint design values according to the same frequency hypothesis that
 274 considering two correlated variables follow the same cumulative probability in their distributions, but this
 275 approach lacks a statistical basis and poorly describes the physical characteristics of droughts (Yin et al.,
 276 2018). In this paper, the joint probability density is used to optimize the most likely realization, which is
 277 mathematically expressed as follows:

278
$$\left\{ \begin{array}{l} (d^*, s^*) = \arg \max f(d, s) = c[F_d, F_s] \cdot f_d \cdot f_s \\ C[F_d, F_s] = 1 - \mu / T_{or} \\ c[F_d, F_s] = \frac{dC(F_d, F_s)}{d(F_d)d(F_s)} \end{array} \right. \quad (14)$$

279 where $c[F_d, F_s]$ is the Copula probability density function; f_d and f_s are the fitted probability density
 280 functions of D and S , respectively; F_d and F_s are the marginal distribution of D and S , respectively; (d^*, s^*)

281 is the most likely realization under a given JRP T_{or} ; μ is the mean inter-arrival time between two
 282 consecutive droughts.



283 **Figure 3. Joint distribution of drought duration and severity under a critical T_{or} .** The green lines are two arbitrary
 284 values of duration and severity. The red line is the isoline line of two variables under a critical T_{or} , and the blue
 285 line denotes the traditional equal-frequency assumption. The d_T and s_T are marginal distribution quantiles for a
 286 given probability level T ; F_S and F_D are cumulative probability density of severity and duration, respectively. T_{or}
 287 is a given probability level under the OR case.
 288

289

290 The future socioeconomic exposure after 2020s has directly been defined as ranging from 0 to 100%
 291 (Gu et al., 2020a), but dynamically shifting climate risks cannot be represented under this definition, without
 292 considering fluctuation in the frequency of hazards. Here, the socioeconomic exposure is defined by
 293 considering the shift in JRP, and is expressed at the catchment scale as follows:

294
$$E_{POP} = \frac{T_h I(T_h - T_f)}{T_f A_d} \times POP \quad (15)$$

295
$$E_{GDP} = \frac{T_h I(T_h - T_f)}{T_f A_d} \times GDP \quad (16)$$

296 where E_{POP} and E_{GDP} denote the population and GDP exposure; T_h and T_f denote the historical and future
 297 JRP, respectively; $I(\cdot)$ denotes the controlling function, which is 1 when $T_h - T_f < 0$, or 0 when
 298 $T_h - T_f \geq 0$ is recorded; POP and GDP denote the population and the gross domestic product (in USD) of a

299 given catchment in the future climate, respectively.

300 **2.6 Quantifying the uncertainty contributed by different sources**

301 Uncertainties in the future drought projections can arise from the SSPs, GCMs and HTMs. During both
302 historical (1985-2014) and future periods (2071-2100), the combination of 3 SSPs, 5 GCMs and 10 HTMs
303 through the impact modeling chain resulted in 150 hybrid combinations. The overall uncertainty is calculated
304 from the variance of the future estimated JRP relative to the historical 50-year droughts. To partition the
305 uncertainty from different sources of data and their interaction effects, the MANOVA is used and expressed
306 as follows (Weinfurt, 1995):

$$307 \quad \Delta y_{x,y,z} = M + S_x + G_y + H_z + I_{x,y,z} \quad (17)$$

308 where M denotes the mean change of all indicators in models; S_x , G_y and H_z denote the impact on
309 indicators of the x^{th} SSP, y^{th} GCM and z^{th} HTM, respectively; $I_{i,j,k}$ is the overall impact arising from the
310 interactions of different sources. The overall variance V is then expressed as follows:

$$311 \quad V = VS + VG + VH + VI_{SG} + VI_{SH} + VI_{GH} + VI_{SGH} \quad (18)$$

312 where VS , VG , VH are the variance from the SSPs, GCMs and HTMs, respectively. VI_{SG} , VI_{SH} , VI_{GH}
313 and VI_{SGH} denote the variance caused by the coupling between different sources of data. The contribution
314 of each source to the overall uncertainty is quantified by the variance of each source to the total variance.

315 **3. Data and materials**

316 **3.1 In situ observation dataset**

317 We use a gridded meteorological dataset with $0.5^\circ \times 0.5^\circ$ resolution, including daily temperature
318 (maximum, minimum and average, °C) and daily precipitation (mm) from 1961 to 2018, provided by the
319 National Meteorological Bureau of China. The dataset is regarded as the latest gridded meteorological dataset
320 in China and has been applied to some studies (e.g., Wu et al., 2018; Yin et al., 2021a,b). Meanwhile, we
321 gathered the daily streamflow of 463 in situ hydrological stations spanning different periods during 1961-
322 2018. The hydrological stations are densely distributed in East China, while West China has a sparser
323 distribution. Through rigorous data quality checks, 179 unnested basins with at least 20 years of data were
324 selected, covering nine major watersheds in China. For more details on streamflow data processing and
325 catchment screening, please refer to Yin et al. (2021b).

326 **3.2 GRACE/GRACE-FO measurements**

327 Temporal variations in the Earth's gravitational field observed by GRACE satellites have been used to

328 retrieve TWS data (Tapley et al., 2004). Many international institutes have released the TWS mascon products
329 at a monthly scale, including the JPL (Jet Propulsion Laboratory of the California Institute of Technology),
330 the GSFC (Goddard Space Flight Center of NASA), and the CSR (Center for Space Research of the
331 University of Texas). As these three mascon solutions are produced at different spatial resolutions, we
332 generated blended TWS data based on the average of JPL, GSFC and CSR with $0.5^{\circ} \times 0.5^{\circ}$ resolution from
333 2002 to 2022, and fill the missing data using a linear interpolation approach (Yin et al., 2022).

334 **3.3 ERA5-Land dataset**

335 ERA5-Land is a dataset that consists of a large volume of meteorological variables, including
336 precipitation, temperature, air pressure etc. The spatial resolution of the dataset is 9 km and the temporal
337 resolution is one hour (Yilmaz, 2023). Under the latest global reanalysis and the lapse rate correction, the
338 ERA5-Land reanalysis dataset provides a substitute for unavailable observed weather data, by taking the
339 effect of altitude on the spatial scheme of climate variables into consideration (Pelosi et al., 2020). Six
340 variables are used in the study (i.e., *pr*, *ps*, T_{2m} , T_d , *srlsds*, *srsds*) and aggregated to a daily scale from the
341 hourly scale before conducting data analysis.

342 **3.4 Bias-corrected GCM outputs and socioeconomic scenarios**

343 The climate outputs of five GCMs of the historical scenario and three SSPs (i.e., SSP1-26, SSP3-70,
344 SSP5-85) under CMIP6 are used to represent different climate scenarios. Generally, the SSP5-85 configured
345 the highest carbon emission and human interference with the natural environment. The SSP3-70 and the
346 SSP1-26 have progressively conservative changes to represent climate change resulting from different levels
347 of human activity. The series of bias-corrected variables have been downscaled to $0.5^{\circ} \times 0.5^{\circ}$ resolution from
348 1850 to 2100 under the Intersectoral Impact Model Intercomparison Project 3b (ISIMIP3b) (Lange, 2019).
349 To reduce the systematical biases of CMIP6 raw outputs, seven variables from the bias-corrected ISMIP3b
350 dataset have been used, namely temperature (daily average, maximum and minimum), *pr*, *ps*, *srsds*, *srlsds*,
351 *RH* and *SH*.

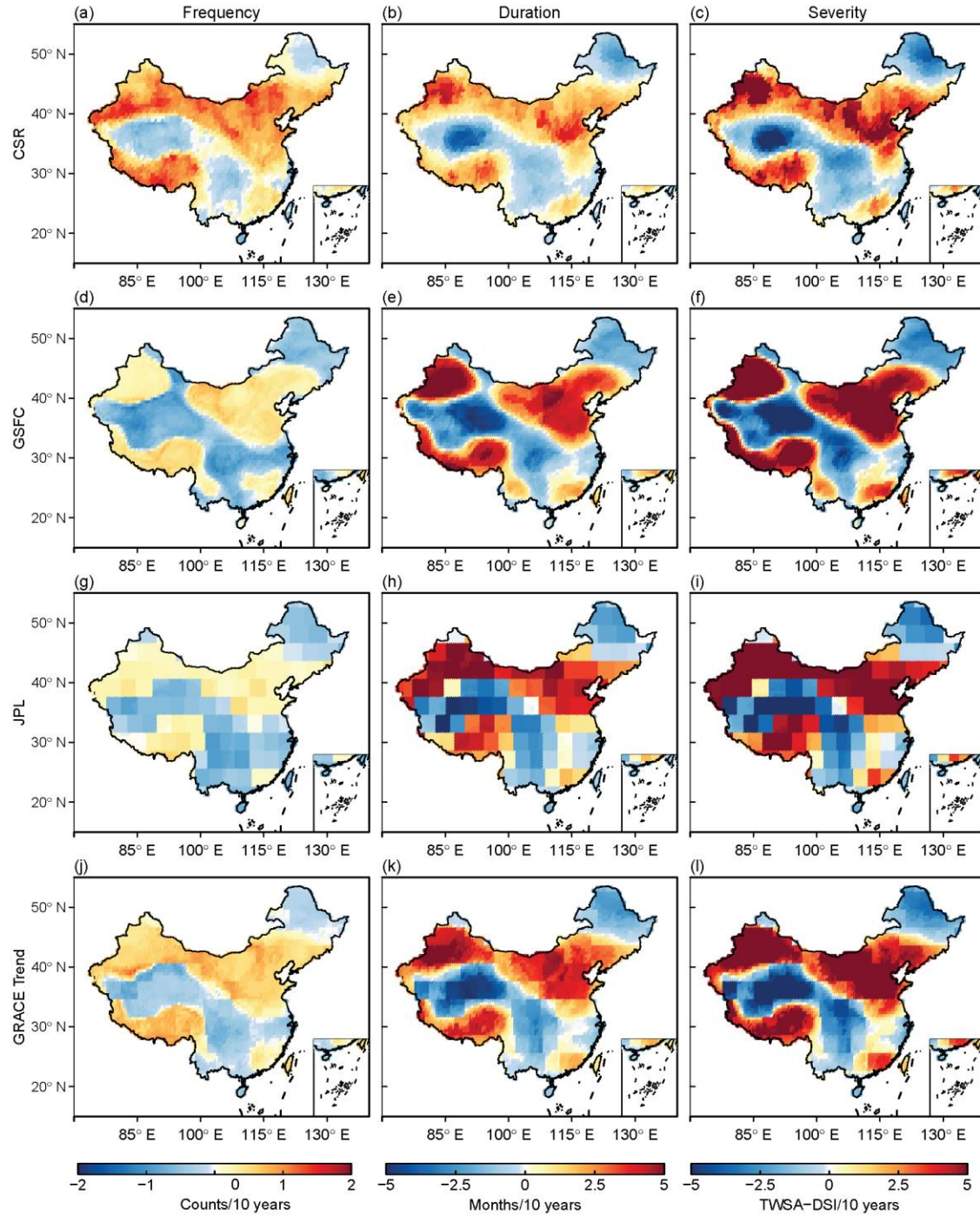
352 Population and GDP data under three SSPs are employed to evaluate the potential socioeconomic risks
353 of drought in a warming world. An open-access population dataset is adopted which takes into consideration
354 the universal two-child policy, the census results and the statistical annual report (Jiang et al., 2017). The
355 economic index from 2010 to 2100 is estimated based on the Cobb-Douglas and Population-Environment-
356 Development model (Jiang et al., 2018). All of the data have been previously used to assess the socio-
357 economic impact of extreme hydrologic hazards (Yin et al., 2022; Yin et al., 2023).

358 **4. Results**

359 **4.1 Observed changes in SRI and TWS-DSI based drought**

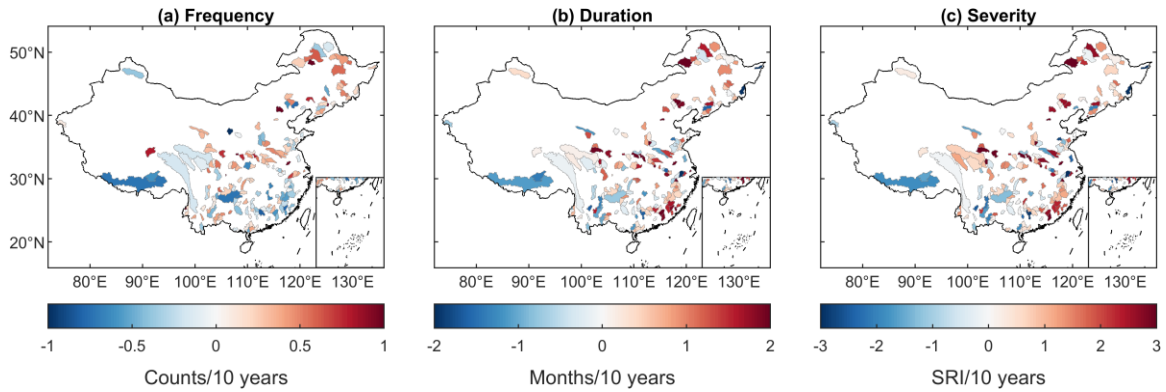
360 As there are insufficient streamflow observations to compute the SRI in northwest China, we also

361 employed the TWS-DSI as a supplement. This approach enriches the variety of water storage or flux being
362 evaluated. Based on linear regression and least square method, trends in drought characteristics (i.e.,
363 frequency, duration and severity) are estimated by using the GRACE/GRACE-FO dataset and observed
364 runoff across China. Figure 4 and Figure 5 show the drought trends based on the TWS-DSI and SRI,
365 respectively. Overall, the two indexes show similar trends in most catchments, suggesting that drought
366 hazards have increased during 2002-2022. TWS-DSI droughts have increased in 54% of areas, which are
367 mainly located in the Qinghai-Tibet Plateau, the North China Plain and the northwestern Xinjiang Province.
368 Likewise, SRI droughts have increased over 51% of studied catchments, which mainly dominate northeastern
369 and southeastern China. The severity of droughts measured by the TWS-DSI index is twice of the
370 hydrological drought, primarily because the TWS-DSI metric incorporates all vertical water fluxes, offering
371 a comprehensive view of shifts in water scarcity. On the other hand, TWS-DSI can difficultly represent the
372 aquifer recharge processes, which are fundamental physical process of baseflow and the hydrological drought
373 in its entire extension. Therefore, catchments with aquifer recharge and storage capacity will exceed several
374 times the time step of the analysis, enlarging the severity of droughts. Some locations exhibit discrepancies
375 depending on the index considered. For instance, droughts in the Qinghai-Tibet Plateau and Northeast China
376 show opposite trends. Anomalies in the Qinghai-Tibetan plateau may be explained by the transformation of
377 snowpack melt into surface runoff under the influence of climate change, which helps compensate for the
378 lack of surface water in the area (Stewart, 2009). The discrepancy observed in Northeastern China could
379 potentially be linked to the rise in soil moisture from increased infiltration, which causes a higher proportion
380 of water to be stored within the soil than at the surface, interfering with the quantification of hydrological
381 drought (Wang et al., 2017). Finally, both indicators show a consistent positive drought trend in most areas
382 of China and particularly the North China Plain and Pearl River Basin.



383
384
385

Figure 4. Trends in drought frequency, duration and severity based on the TWS-DSI from 2002 to 2022 using three GRACE/GRACE-FO products (a-i) and the blended data (j-l).



386

387

388

Figure 5. Trends in drought frequency, duration and severity from 2002 to 2022 over China. (c), the index of severity is based on the SRI statistic (Eq. 13).

389

4.2 Machine Learning-constrained streamflow simulation and model evaluation

390

391

392

393

394

395

396

397

398

399

400

401

402

403

404

405

406

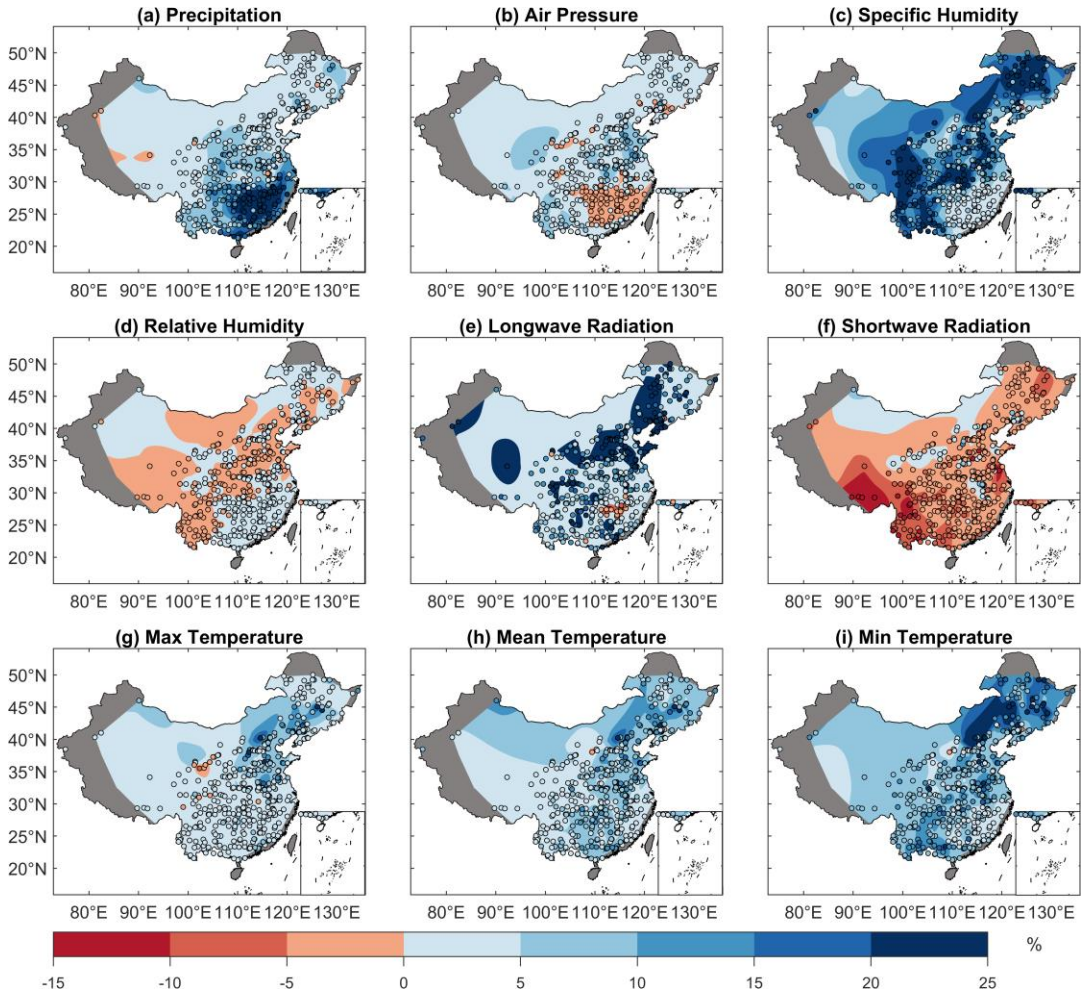
407

408

409

410

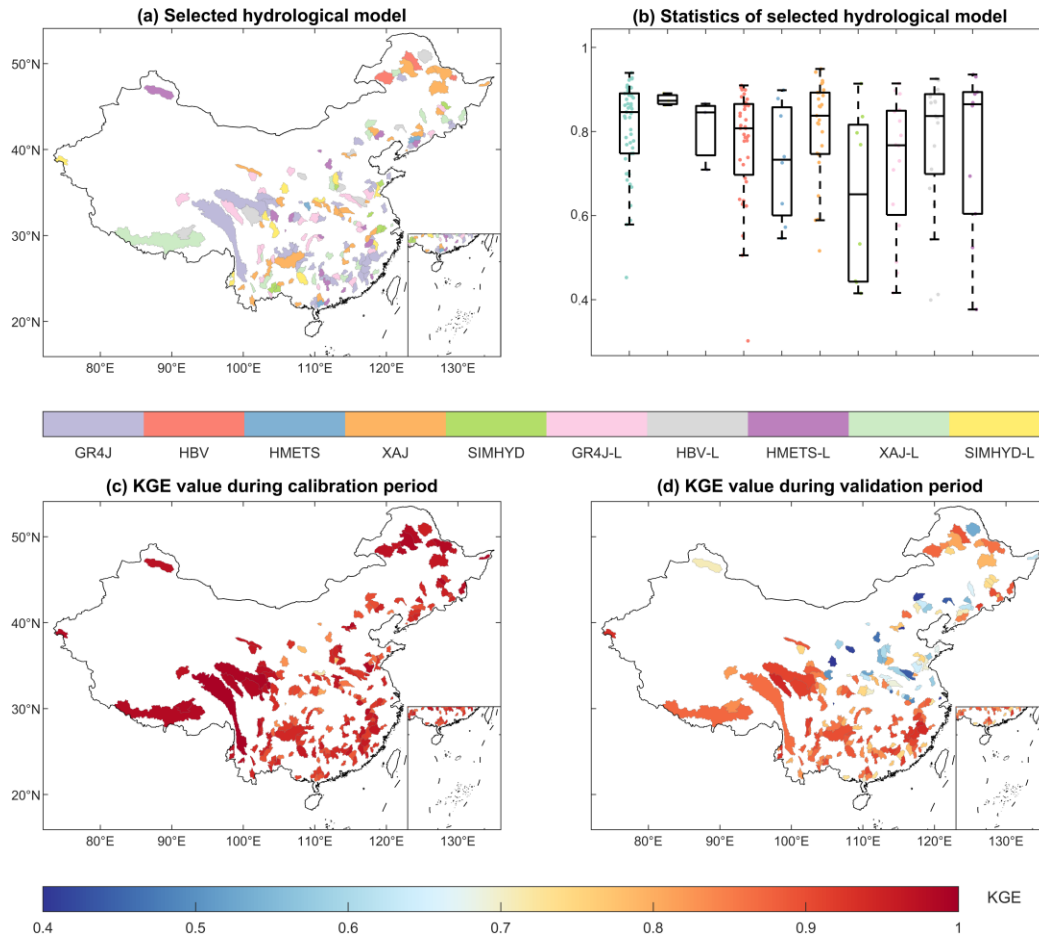
The RF model was used to quantify the sensitivity of streamflow to different meteorological variables (Figure 6). Since a station can be attributed to catchments of different sizes, we only considered the largest catchment scales in analysis. We quantified the sensitivity of seven historical mean meteorological variables (i.e., *pr*, *ps*, *SH*, *RH*, *srls*, *srsds*, temperature) to monthly streamflow in each grid. Due to the sparse number of observation stations in Northwestern China, the reliability of the sensitivity analysis for these regions is lower than that of the dense observed areas. Precipitation typically plays a major role in generating runoff in Southeast China, although *SH* plays the most important role in some regions such as Central, Southwest and Northeast China. Over 30% and 38% of stations show the *SH* sensitivity rate of >10% in Western and Northeastern China respectively, indicating the dominance of *SH* in these areas. In contrast, *RH* and shortwave radiation have a negative contribution to streamflow; especially shortwave radiation, which has a pronounced negative sensitivity in 394 stations probably due to enhanced evapotranspiration (Ma et al., 2019). These negative contributions mean enhancement of these two variables will inhibit the generation of streamflow, showing the potential adverse effects of climate change on streamflow generation. In general, *RH* contributes to increasing streamflow over most regions of China, but the opposite effect is observed in 179 stations mainly located in Southwestern China, Yellow River and Huaihe River basins. This is the result of the mutual feedback of water and heat dynamics (i.e., saturated vapor pressure increases with warming and intensifies evaporation, leading to a decrease in surface water), which was also found by Liu et al. (2017). The temperature has a positive contribution to streamflow generation in Northeast China, suggesting a potential mitigation for the deficiency of surface flow. However, there is interactive feedback between hydrological and thermal factors that result in an inability to directly assess the impact of temperature on hydrologic droughts (Fig. 6i and 6f).



411

412 **Figure 6. Sensitivity of meteorological variables to daily streamflow. The figure uses a thin plate smoothing spline**
 413 **method to interpolate the point-based station data (circles). Gray areas indicate missing data.**

414 The performances of simulated streamflow by different HTMs are shown in Figure 7. The model that
 415 has the largest Kling-Gupta efficiency (KGE) is considered to be the best-performing in each catchment. In
 416 Fig 7. (a) and (b), the GR4J and GR4J-LSTM performed best in 77 out of 179 studied catchments. The
 417 median KGE value of GR4J is higher than 0.83, revealing a superior performance than the other hydrological
 418 models. Subsequently, the XAJ and XAJ-LSTM are the best models in 57 catchments, mainly located in the
 419 southern Yangtze River. Last, the HBV and HBV-LSTM performed best in only 10 catchments, where the
 420 streamflow are impacted by snowfall in plateaus and northern frozen areas. All catchments exhibit KGE
 421 values greater than 0.9 during the calibration period in Figure 7c, showing good performance in simulation.
 422 During the validation period, only 18 catchments have KGE values below 0.6, and most of the catchments
 423 have KGE values greater than 0.8 in Figure 7d. In summary, the trained models simulate streamflow well in
 424 all the studied catchments. Additionally, the KGE values in the southern region are generally higher than
 425 those in the northern region during the validation period, which is consistent with previous hydrological
 426 simulation works (Gu et al., 2020b, 2021). This phenomenon may be attributed to the higher dependence of
 427 streamflow on rainfall in South China, which is governed by a humid climate pattern (Zheng et al., 2022).



428

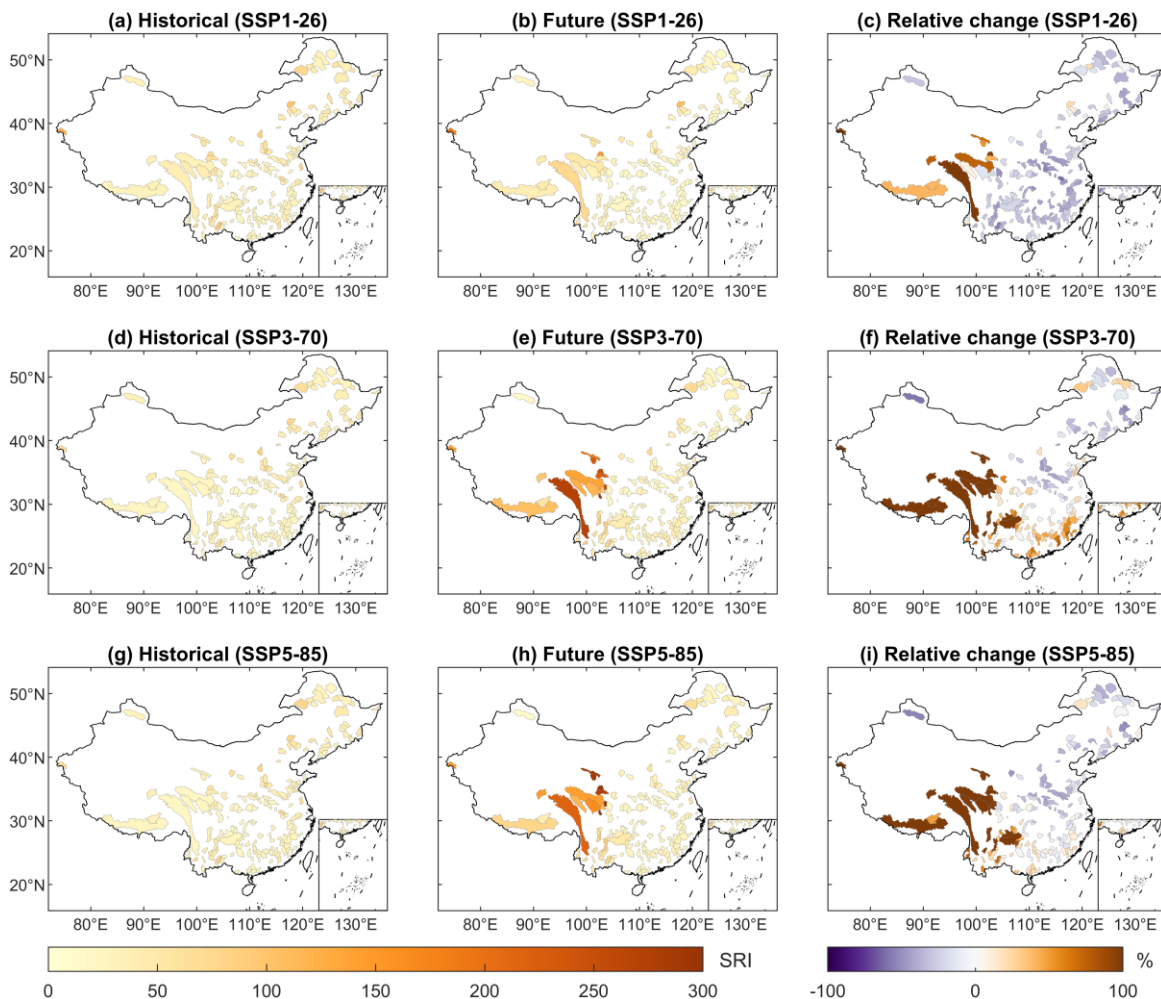
429 **Figure 7. Hydrological simulation performances of all candidate models. (a), The best-performing model with the**
 430 **highest KGE value. The catchments are colored according to the best performing models. (b), Boxplots of all**
 431 **catchments for ten HTMs indicated by KGE values. (c)-(d), The highest KGE values during the calibration (c)**
 432 **and validation (d) period, respectively.**

433 4.3 Projected changes in univariate drought characteristics

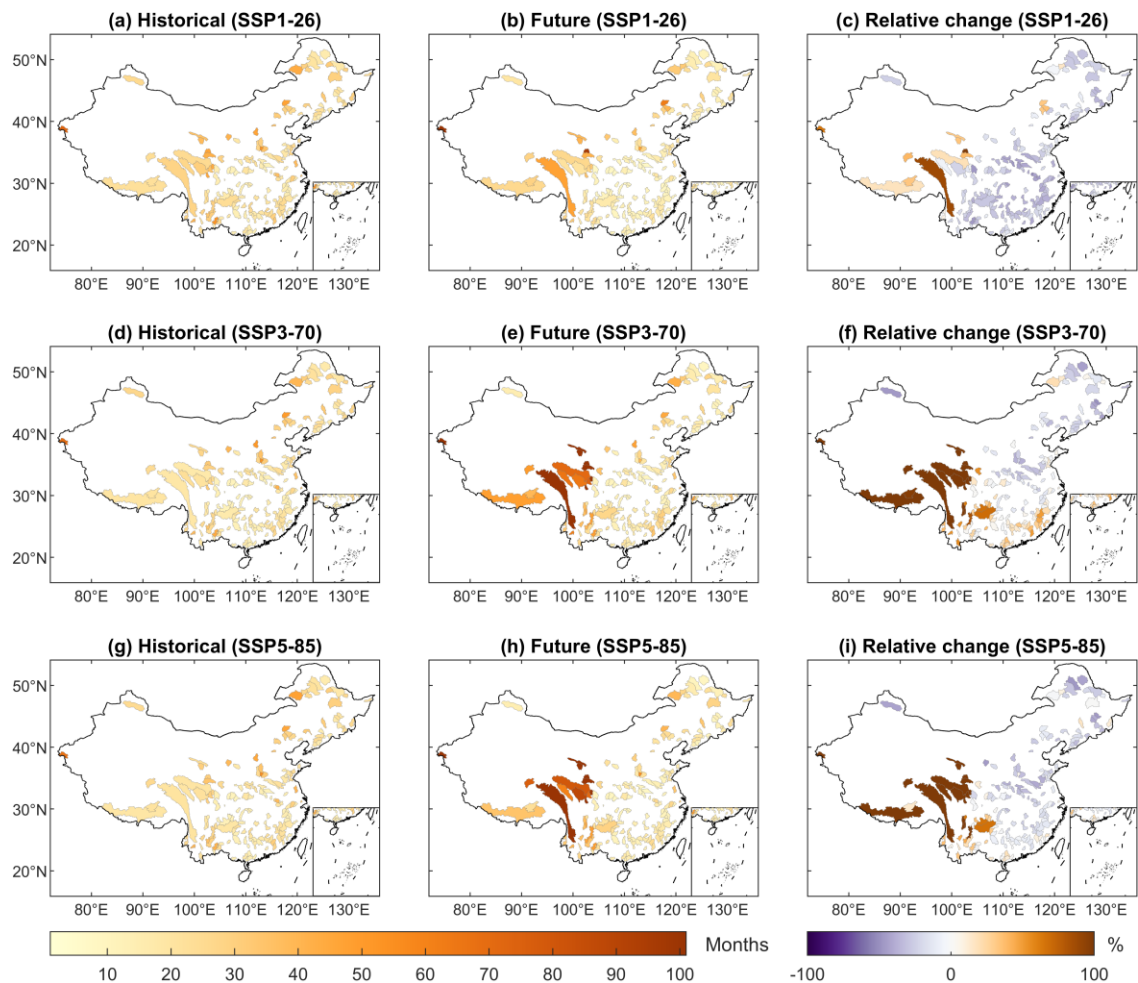
434 We projected the future daily runoff series by driving the HTMs with the bias-corrected CMIP6 variables,
 435 and then we estimated the monthly SRI to identify drought duration and severity. Based on the maximum
 436 Bayesian Information Criterion (BIC), we selected the best-performing marginal distributions for duration
 437 and severity from seven candidate distributions shown in Table S2, based on historical data for each
 438 catchment. Figure 8 and Figure 9 show the multi-model ensemble average severity and duration for the 50-
 439 year historical return period (RP).

440 In western China, we projected a significantly increasing drought trend under the three SSPs, which
 441 indicates potential for increased water scarcity and more frequent extreme drought events. In Southeast China,
 442 we projected that drought events are likely to intensify under SSP3-70 but not under SSP5-85. It is generally
 443 considered that SSP5-85 is accompanied by higher carbon emissions than that of SSP3-70 (O'Neill et al.,
 444 2016). However, future works also take significant action to control the extent of climate change combined
 445 with strong climate policies under SSP5-85 (Fujimori et al., 2017). As a result, there is no deterioration of

446 drought severity with policy interventions, which emphasizes the significance of ensuring the implementation
 447 of climate strategies. In northern China, in contrast, we found that future drought risks are projected to
 448 decrease under the three scenarios, which is possibly related to more moisture convergence from the East
 449 Asian monsoon circulation as the warming climate (Chowdary et al., 2019).

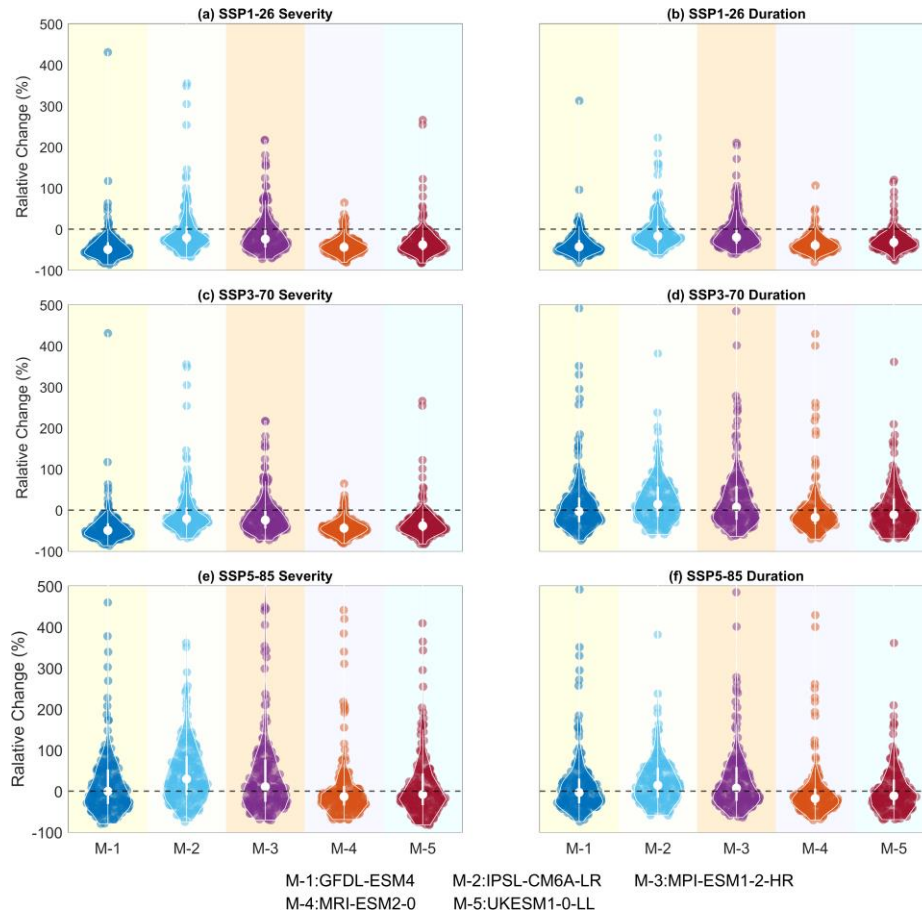


450
 451 **Figure 8. Multi-model ensemble average design severity (dimensionless) under a 50-year RP for three SSPs, and**
 452 **relative changes (%) in 2071-2100 compared to 1985-2014.**



453
 454 **Figure 9. Multi-model ensemble average design duration (months) of the multi-model for a 50-year RP for three**
 455 **SSPs, and relative changes (%) in 2071-2100 compared to 1985-2014.**

456 We display the relative change of drought characteristics under 50-year RP for all catchments for five
 457 GCMs under the three SSPs using violin plots (Figure 10). For most catchments, the relative change of
 458 drought duration and severity is negative. However, the relative change under some scenarios reached a
 459 maximum of 400%, highlighting the extreme change of drought. The median relative change of severity
 460 based on the IPSL-CM6A-LR under SSP3-70 are 30%, and 22% of catchments have a relative change over
 461 200%, representing the most severe case of drought evolution. Furthermore, the distributions of the
 462 projections based on the MPI-ESM1-2-HR, MRI-ESM2-0 and UKESM1-0-LL models are highly skewed
 463 and bimodal under SSP3-70 and SSP5-85, revealing substantial spatial heterogeneity across China. Overall,
 464 the severity and duration of droughts slightly increase in some catchments and have the risk of extreme
 465 intensification as a result of global warming.



466

467 **Figure 10. Violin plots of relative changes (%) in severity and duration to the historical drought event with 50-**
 468 **year RP under three SSPs. The white circles are the median values of relative changes.**

469

4.4 Bivariate drought changes and corresponding socioeconomic risks

470

471

472

473

474

475

476

477

478

479

480

481

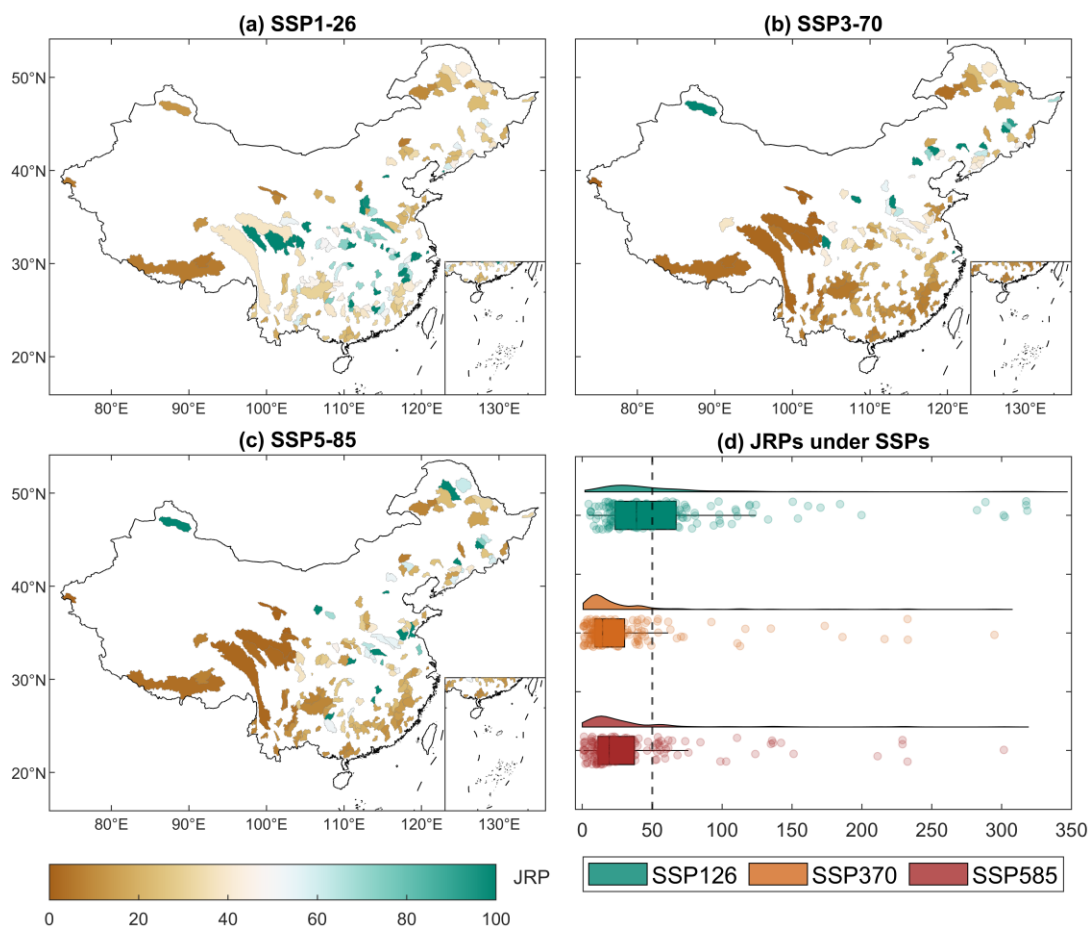
482

483

To capture the complex dependence structure between drought severity and duration, we used a Copula function to quantify the bivariate risk of hydrological droughts under climate change. Changes in the JRP of the historical (1985-2014) drought event with 50-year JRP in the future (2071-2100) period are shown in Figure 11. The medians of the projected future JRP are 38.78 years, 14.52 years and 19.24 years under SSP1-26, SSP3-70 and SSP5-85, respectively. For 69% and 60% catchments under SSP3-70 and SSP5-85, we find the JRP of the 50-year drought is reduced to less than 25 years in the future period, suggesting that the risk of drought increases over 2 times in these catchments. Besides, we find a marked increase in the number of catchments with increased drought risk compared to the univariate drought assessments. The JRP of catchments in Northeastern and Central China tends to decrease, suggesting higher changes in risks than univariate assessments. This result is consistent with previous studies (He et al., 2011; Xu et al., 2015), which indicates that the use of bivariate drought analysis can amplify the individual effects of two drought characteristics.

Future GDP and population exposed to increasing bivariate drought risk under three scenarios are shown in Figure 12. The eastern coastal regions have a higher significant economic exposure such as the Huaihe

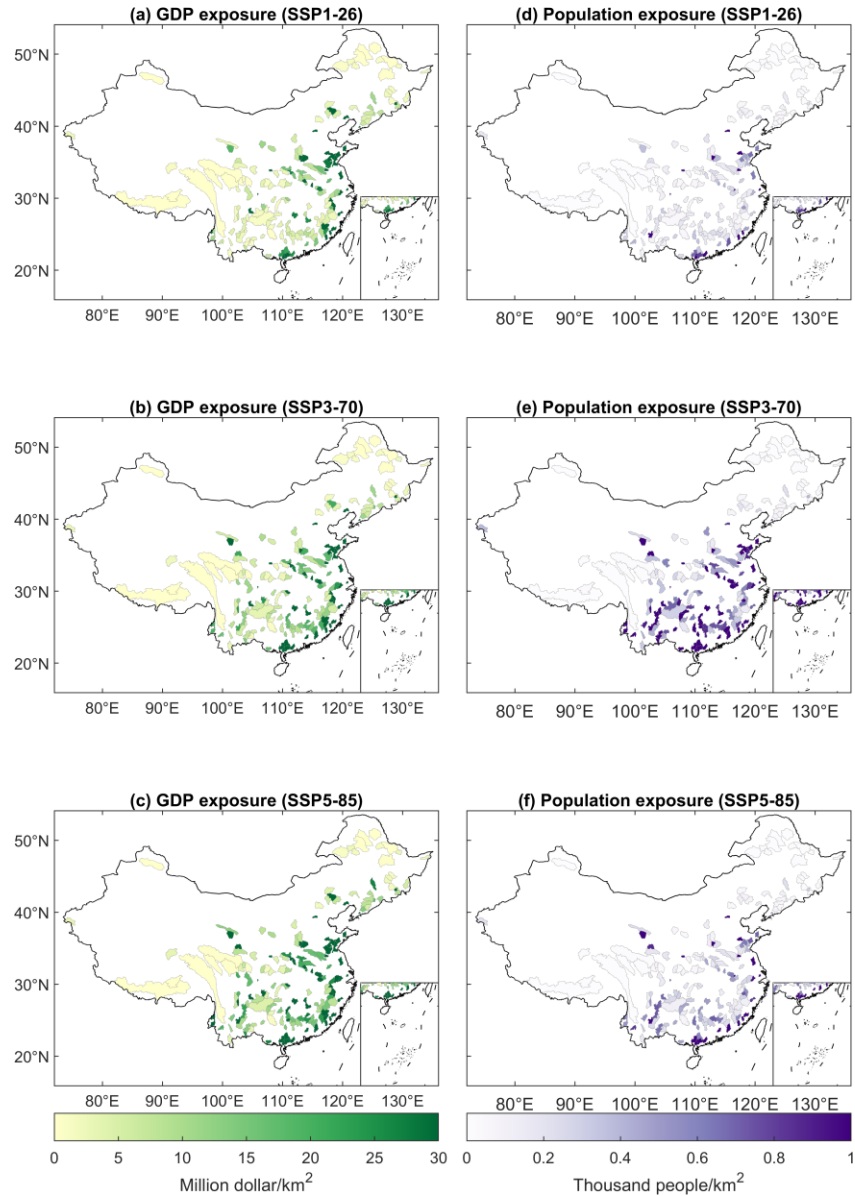
484 River Basin, the Yangtze River Basin and the Pearl River Basin, which is consistent with the distribution of
 485 economically developed regions in China. The medians of GDP exposure are 5.5, 9.8 and 14.3 million
 486 dollars/km² under three SSPs respectively, which indicates the vulnerability of economic losses to drought
 487 disasters under global warming. The population affected by drought is mainly located in the southern Yangtze
 488 River Basin and the Huaihe River Basin under SSP3-70, as the median exposure is 525 and 205 people/km²
 489 under SSP3-70 and SSP5-85, respectively. This is because the increase in population is higher in the Sichuan,
 490 Guangdong and Zhejiang provinces than in other Chinese provinces under SSP3-70 (Chen et al., 2020).
 491 Overall, the exposure of GDP and population shows large heterogeneity in their sensitivity to different
 492 scenarios, and the distribution of the affected catchments is consistent with economic and social development.



493

494 **Figure 11. The future multi-model ensemble means JRP of the historical drought with a 50-year T_{or} based on the**
 495 **bivariate approach. The future JRPs of 179 catchments under three SSPs are presented in (a)-(c), while (d)**
 496 **displays raincloud plots of the projected JRP under each SSP.**

497



498

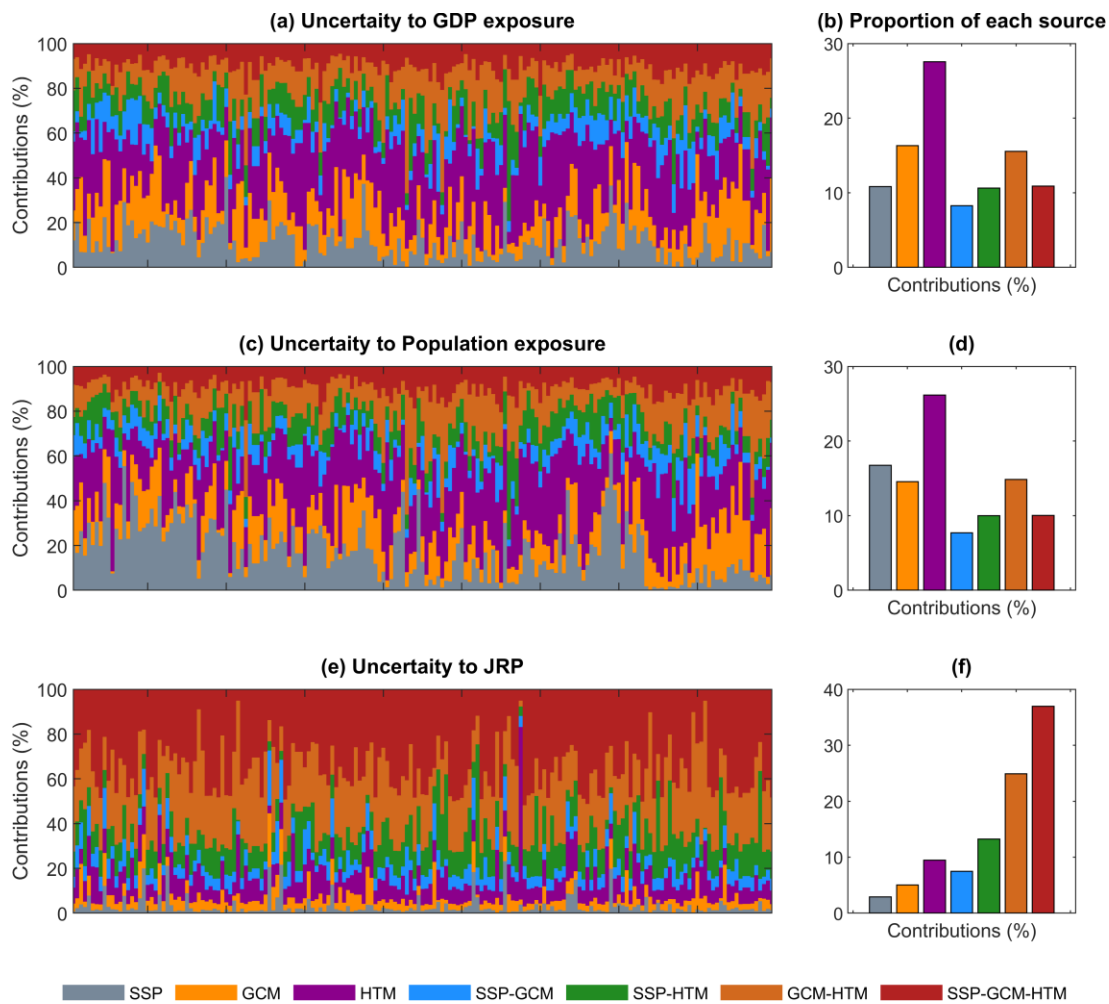
499 **Figure 12. The multi-model ensemble means exposure of GDP (a-c) and population (d-f) to bivariate drought**
 500 **characteristics under different SSPs in the future period.**

501 **5. Discussion**

502 **5.1 Uncertainty decomposition**

503 The overall uncertainty in our projections arises from the different SSPs, GCMs and HTMs as well as
 504 their interactions. We assemble these seven sources using MANOVA (Figure 13). For GDP and POP exposure,
 505 we find HTM is the main source of uncertainty, and contributes 27.55% and 26.14% uncertainty, respectively.
 506 This indicates that the quality of the HTM is important for the accuracy of socioeconomic predictions.
 507 Likewise, the GCM and GCM-HTM provide over 30% of the uncertainty in GDP and population exposures,

508 which indicates the critical importance of bias-corrected GCM outputs for accurate projections. Further, the
 509 contributions of the SSPs to population exposure is 1.5 times than that of GDP exposure, which shows that
 510 the effect of climate change is greater for POP exposure than GDP exposure. In particular, the independent
 511 factors (i.e., SSP, GCM, HTM) contribute over 50% to the uncertainty of GDP and population exposures,
 512 suggesting that GDP and population exposures are less responsive to complex coupling. In contrast, the
 513 coupled factors (i.e., the combination of SSP, GCM or HTM) mainly contribute to the uncertainty of the JRP,
 514 accounting for 82.63% of the overall uncertainty, especially the SSM-GCM-HTM, which accounts for 36.97%
 515 of uncertainty. Finally, the relatively low contribution of the choice of SSP, SSP-GCM and SSP-HTM to JRP
 516 uncertainty indicates that the future risk projection uncertainty is relatively stable in future risk projections



517
 518 **Figure 13. The fractional uncertainty contributions of all sources to the GDP exposure, population exposure, and**
 519 **JRP estimate for all 179 catchments (a, c, e) and the average fractional contribution of each source (b, d, f).**

520 5.2 Limitations and future work

521 The uncertainty caused by the underlying surface situation and the coupling relationships behind
 522 interrelated variables remains unexplained in this study. Therefore, revealing interactions among multisource
 523 data is important to understand how the drivers affect the water cycle under climate change. Here, only five

524 GCM outputs and one in situ observation dataset were used to drive our HTM models. The sparse dataset
525 may undermine the robustness of the approach. Providing a larger number of GCMs and observational data
526 to assemble a more sophisticated model might be an effective approach to improve accuracy and reliability.
527 Although the catchments gathered in this study cover nine major watersheds in China, there is still a
528 requirement for streamflow data with a more uniform spatial density. Considering geospatial sampling
529 techniques, a homogeneous density of catchments is significant to reveal the spatial distribution of drought.
530 On the other hand, due to the heterogeneity of different climatic regions in China, we would like to expand
531 hydrological models (e.g., the weather research and forecasting model hydrological modeling system, soil
532 and water assessment tool or the hydrological modules of land surface process models) to reduce uncertainty
533 in future research. Finally, the GDP and population projections cannot well reflect future economic
534 development and population migration, especially the governmental intervention in immigration and
535 economic policies. It is better to consider the dynamic impact of human management on socioeconomic
536 development, which is essential for the construction of a more reliable projection framework.

537 **5.3 Suggestions for drought mitigation in China**

538 In order to curb global warming and mitigate the threats of climate change, the Chinese government is
539 striving to reach its carbon peak before 2030, achieve carbon neutrality before 2060, and bolster efforts in
540 disaster reduction (Kundzewicz et al., 2019; Liu et al., 2022b). China has nonetheless experienced several
541 extreme drought events during the past 5 years, threatening the population's health and economic
542 development (Ding and Gao, 2020; Liu et al., 2022a; Mallapaty, 2022). The Intergovernmental Panel on
543 Climate Change (IPCC) has emphasized that projections of future climate trends can equip policymakers
544 with the scientific insight needed to navigate the challenges of climate change (Pörtner et al., 2022). The
545 results of this study aim to alert policymakers to drought risk in Southwestern China which was just hit by
546 severe drought events and expected to significantly intensify with climate change. We strongly highlight the
547 importance of strictly implementing carbon emission reduction initiatives and developing prevention
548 programs to limit potential drought losses. Preserving local ecological balance and employing rational use of
549 water resources could be the key to mitigating potential losses from extreme droughts (Chang et al., 2019;
550 Sohn et al., 2016). Although China has constructed hydraulic structures with a total water storage capacity of
551 over 7,064 billion m³, current irrigation facilities need to expand to mitigate the challenge of drought under
552 climate change (Cai et al., 2015; Xiao-jun et al., 2012). In addition, it is also beneficial for policymakers that
553 establish a drought information system to get a comprehensive collection of drought impacts from all
554 potential sectors, which can link the government and research organizations (Wilhite et al., 2007).

555 The Intergovernmental Panel on Climate Change (IPCC) has emphasized that projections of future
556 climate trends can equip policymakers with the scientific insight needed to navigate the challenges of climate
557 change (Pörtner et al., 2022). The results of this study aim to alert policymakers to drought risk in
558 Southwestern China, which is expected to intensify with climate change. Preserving local ecological balance
559 and employing rational use of water resources could be the key in mitigating potential losses from extreme

560 droughts (Chang et al., 2019; Sohn et al., 2016). Finally, this work highlights the importance of strictly
561 implementing carbon emission reduction initiatives and developing prevention programs to limit potential
562 drought losses.

563 **6. Conclusions**

564 In this study, the hybrid LSTM-constrained hydrological models show high efficiency in studied
565 catchments over China, demonstrating that machine learning can effectively constrain the hydrological
566 simulation. Projected changes in 50-year bivariate drought characteristics, expressed as a JRP, indicate that
567 the risk of hydrological drought is likely to more than double in over 60% of catchments by the end of the
568 21st century under SSP5-85. The spatial distribution of change reveals that the catchments with severely
569 increased drought risk are mainly located in southwestern China. Notably, the exposure of GDP and
570 population varies greatly across different SSPs. The median GDP exposure under SSP5-85 is 1.5 times that
571 of SSP3-70, but the median population exposure is just 40% that of SSP3-70. The higher population exposure
572 under SSP3-70 can be attributed to rapid population growth. Finally, we find the interaction between multiple
573 sources of data explains more than 80% of the uncertainty in future changes in JRPs, showing the importance
574 of considering the relationships between model components. Our findings demonstrate that China will face
575 higher drought risks in a warmer future, emphasizing the urgency of implementing strategies to reduce carbon
576 emissions. Our study is insufficient in the revelation of drought hazard drivers and needs to expand datasets
577 and hydrological models to promote the reliability of simulation in future studies. We would also like to take
578 governmental interference of economic and demographic policies into consideration.
579

580 **Data availability**

581 The gridded meteorological dataset for China can be obtained from <http://www.cma.gov.cn>. The
582 ISIMIP3b data can be downloaded from <https://data.isimip.org>. The ERA5-Land data can be
583 downloaded from <https://www.ecmwf.int/en/era5-land>. Streamflow simulations used in this study
584 are available at <https://osf.io/fvyse/>.

585 **Acknowledgments**

586 J.Y. acknowledges support from the National Natural Science Foundation of China (Grant NOs.
587 52361145864; 52261145744). L.S. is supported by UKRI (MR/V022008/1). J.G. is supported by the
588 National Natural Science Foundation of China (NO. 52179018). This work is also supported by the
589 Undergraduate Training Programs for Innovation and Entrepreneurship of Wuhan University. The
590 numerical calculations in this paper have been performed on the supercomputing system in the
591 Supercomputing Center of Wuhan University.

592 **Competing interests**

593 At least one of the (co-)authors is a member of the editorial board of Hydrology and Earth System
594 Sciences.

595 **References**

- 596 Allan, R. P., Barlow, M., Byrne, M. P., Cherchi, A., Douville, H., Fowler, H. J., Gan, T. Y., Pendergrass,
597 A. G., Rosenfeld, D., Swann, A. L. S., Wilcox, L. J., and Zolina, O.: Advances in understanding
598 large-scale responses of the water cycle to climate change, *Annals of the New York Academy of*
599 *Sciences*, 1472, 49–75, <https://doi.org/10.1111/nyas.14337>, 2020.
- 600 Antoniadis, A., Lambert-Lacroix, S., and Poggi, J.-M.: Random forests for global sensitivity analysis: A
601 selective review, *Reliability Engineering & System Safety*, 206, 107312, 2021.
- 602 Arsenaault, R., Essou, G. R., and Brissette, F. P.: Improving hydrological model simulations with combined
603 multi-input and multimodel averaging frameworks, *Journal of Hydrologic Engineering*, 22, 04016066,
604 2017.
- 605 Ashrafi, S. M., Gholami, H., and Najafi, M. R.: Uncertainties in runoff projection and hydrological drought
606 assessment over Gharezu basin under CMIP5 RCP scenarios, *Journal of Water and Climate Change*,
607 11, 145–163, 2020.
- 608 Ayantobo, O. O., Li, Y., Song, S., and Yao, N.: Spatial comparability of drought characteristics and related
609 return periods in mainland China over 1961–2013, *Journal of Hydrology*, 550, 549–567, 2017.
- 610 Barker, L. J., Hannaford, J., Chiverton, A., and Svensson, C.: From meteorological to hydrological drought
611 using standardised indicators, *Hydrology and Earth System Sciences*, 20, 2483–2505, 2016.
- 612 Bergström, S.: The HBV model, *Computer models of watershed hydrology*, 443–476, 1995.
- 613 BERGSTRÖM, S. and FORSMAN, A.: DEVELOPMENT OF A CONCEPTUAL DETERMINISTIC
614 RAINFALL-RUNOFF MODEL, *Hydrology Research*, 4, 147–170, 1973.
- 615 Berne, A., Delrieu, G., Creutin, J.-D., and Obled, C.: Temporal and spatial resolution of rainfall
616 measurements required for urban hydrology, *Journal of Hydrology*, 299, 166–179, 2004.
- 617 Byakatonda, J., Parida, B. P., Moalafhi, D. B., and Kenabatho, P. K.: Analysis of long term drought
618 severity characteristics and trends across semiarid Botswana using two drought indices, *Atmospheric*
619 *research*, 213, 492–508, 2018.
- 620 Cai, X., Zeng, R., Kang, W. H., Song, J., and Valocchi, A. J.: Strategic Planning for Drought Mitigation
621 under Climate Change, *Journal of Water Resources Planning and Management*, 141, 04015004,
622 [https://doi.org/10.1061/\(ASCE\)WR.1943-5452.0000510](https://doi.org/10.1061/(ASCE)WR.1943-5452.0000510), 2015.
- 623 Castle, S. L., Thomas, B. F., Reager, J. T., Rodell, M., Swenson, S. C., and Famiglietti, J. S.: Groundwater
624 depletion during drought threatens future water security of the Colorado River Basin, *Geophysical*
625 *research letters*, 41, 5904–5911, 2014.
- 626 Catani, F., Lagomarsino, D., Segoni, S., and Tofani, V.: Landslide susceptibility estimation by random
627 forests technique: sensitivity and scaling issues, *Natural Hazards and Earth System Sciences*, 13,
628 2815–2831, <https://doi.org/10.5194/nhess-13-2815-2013>, 2013.
- 629 Chang, J., Guo, A., Wang, Y., Ha, Y., Zhang, R., Xue, L., and Tu, Z.: Reservoir operations to mitigate
630 drought effects with a hedging policy triggered by the drought prevention limiting water level, *Water*
631 *Resources Research*, 55, 904–922, 2019.
- 632 Chen, H. and Sun, J.: Increased population exposure to extreme droughts in China due to 0.5 °C of
633 additional warming, *Environ. Res. Lett.*, 14, 064011, <https://doi.org/10.1088/1748-9326/ab072e>, 2019.
- 634 Chen, J., Li, C., Brissette, F. P., Chen, H., Wang, M., and Essou, G. R.: Impacts of correcting the inter-
635 variable correlation of climate model outputs on hydrological modeling, *Journal of hydrology*, 560,
636 326–341, 2018.
- 637 Chen, Y., Guo, F., Wang, J., Cai, W., Wang, C., and Wang, K.: Provincial and gridded population
638 projection for China under shared socioeconomic pathways from 2010 to 2100, *Scientific Data*, 7, 83,
639 <https://doi.org/10.1038/s41597-020-0421-y>, 2020.
- 640 Chen, Z. and Yang, G.: Analysis of drought hazards in North China: distribution and interpretation, *Nat*
641 *Hazards*, 65, 279–294, <https://doi.org/10.1007/s11069-012-0358-3>, 2013.
- 642 Chiew, F. H. S., Peel, M. C., and Western, A. W.: Application and testing of the simple rainfall-runoff
643 model SIMHYD., *Mathematical models of small watershed hydrology and applications*, 335–367,
644 2002.

645 Cho, K., Van Merriënboer, B., Gulcehre, C., Bahdanau, D., Bougares, F., Schwenk, H., and Bengio, Y.:
646 Learning phrase representations using RNN encoder-decoder for statistical machine translation, arXiv
647 preprint arXiv:1406.1078, 2014.

648 Chowdary, J. S., Hu, K., Srinivas, G., Kosaka, Y., Wang, L., and Rao, K. K.: The Eurasian jet streams as
649 conduits for East Asian monsoon variability, *Current Climate Change Reports*, 5, 233–244, 2019.

650 Dai, A., Zhao, T., and Chen, J.: Climate Change and Drought: a Precipitation and Evaporation Perspective,
651 *Curr Clim Change Rep*, 4, 301–312, <https://doi.org/10.1007/s40641-018-0101-6>, 2018.

652 Dikici, M.: Drought analysis with different indices for the Asi Basin (Turkey), *Sci Rep*, 10, 20739,
653 <https://doi.org/10.1038/s41598-020-77827-z>, 2020.

654 Dikshit, A., Pradhan, B., and Huete, A.: An improved SPEI drought forecasting approach using the long
655 short-term memory neural network, *Journal of environmental management*, 283, 111979, 2021a.

656 Dikshit, A., Pradhan, B., and Alamri, A. M.: Long lead time drought forecasting using lagged climate
657 variables and a stacked long short-term memory model, *Science of The Total Environment*, 755,
658 142638, 2021b.

659 Ding, T. and Gao, H.: The record-breaking extreme drought in Yunnan Province, Southwest China during
660 spring-early summer of 2019 and possible causes, *Journal of Meteorological Research*, 34, 997–1012,
661 2020.

662 Dixit, S., Atla, B. M., and Jayakumar, K. V.: Evolution and drought hazard mapping of future
663 meteorological and hydrological droughts using CMIP6 model, *Stochastic Environmental Research
664 and Risk Assessment*, 36, 3857–3874, 2022.

665 Donat, M. G., Lowry, A. L., Alexander, L. V., O’Gorman, P. A., and Maher, N.: More extreme
666 precipitation in the world’s dry and wet regions, *Nature Climate Change*, 6, 508–513, 2016.

667 Duan, Q., Sorooshian, S., and Gupta, V.: Effective and efficient global optimization for conceptual rainfall-
668 runoff models, , 28, 1015–1031, 1992.

669 Fujimori, S., Hasegawa, T., Masui, T., Takahashi, K., Herran, D. S., Dai, H., Hijioka, Y., and Kainuma, M.:
670 SSP3: AIM implementation of shared socioeconomic pathways, *Global Environmental Change*, 42,
671 268–283, 2017.

672 Ganguli, P. and Merz, B.: Trends in compound flooding in northwestern Europe during 1901–2014,
673 *Geophysical Research Letters*, 46, 10810–10820, 2019.

674 Gers, F. A., Schmidhuber, J., and Cummins, F.: Learning to forget: continual prediction with LSTM,
675 *Neural Comput*, 12, 2451–71, 2000.

676 Green, J. K., Berry, J., Ciais, P., Zhang, Y., and Gentine, P.: Amazon rainforest photosynthesis increases in
677 response to atmospheric dryness, *Science Advances*, 6, eabb7232, 2020.

678 Gu, L., Chen, J., Yin, J., Sullivan, S. C., Wang, H.-M., Guo, S., Zhang, L., and Kim, J.-S.: Projected
679 increases in magnitude and socioeconomic exposure of global droughts in 1.5 and 2°C
680 warmer climates, *Hydrology and Earth System Sciences*, 24, 451–472, [https://doi.org/10.5194/hess-
681 24-451-2020](https://doi.org/10.5194/hess-24-451-2020), 2020a.

682 Gu, L., Chen, J., Yin, J., Xu, C.-Y., and Zhou, J.: Responses of precipitation and runoff to climate warming
683 and implications for future drought changes in China, *Earth’s Future*, 8, e2020EF001718, 2020b.

684 Gu, L., Yin, J., Zhang, H., Wang, H.-M., Yang, G., and Wu, X.: On future flood magnitudes and estimation
685 uncertainty across 151 catchments in mainland China, *International Journal of Climatology*, 41, E779–
686 E800, 2021.

687 Gu, L., Yin, J., Wang, S., Chen, J., Qin, H., Yan, X., He, S., and Zhao, T.: How well do the multi-satellite
688 and atmospheric reanalysis products perform in hydrological modelling, *Journal of Hydrology*, 617,
689 128920, <https://doi.org/10.1016/j.jhydrol.2022.128920>, 2023.

690 He, B., Lü, A., Wu, J., Zhao, L., and Liu, M.: Drought hazard assessment and spatial characteristics
691 analysis in China, *Journal of Geographical Sciences*, 21, 235–249, 2011.

692 Hu, C., Guo, S., Xiong, L., and Peng, D.: A modified Xinanjiang model and its application in northern
693 China, *Hydrology Research*, 36, 175–192, 2005.

694 Jiang, T., Chen, Y. D., Xu, C., Chen, X., Chen, X., and Singh, V. P.: Comparison of hydrological impacts
695 of climate change simulated by six hydrological models in the Dongjiang Basin, South China, *Journal
696 of Hydrology*, 336, 316–333, <https://doi.org/10.1016/j.jhydrol.2007.01.010>, 2007.

697 Jiang, T., Jing, Z., Cheng, J., Lige, C., Yanjun, W., Hemin, S., Anqian, W., Jinlong, H., Buda, S., and Run,
698 W.: National and provincial population projected to 2100 under the shared socioeconomic pathways in
699 China, *Advances in Climate Change Research*, 13, 128, 2017.

700 Jiang, T., Jing, Z., Li-Ge, C. A. O., Yan-Jun, W., Bu-Da, S. U., Cheng, J., Run, W., and Chao, G. A. O.:
701 Projection of national and provincial economy under the shared socioeconomic pathways in China,
702 *Advances in Climate Change Research*, 14, 50, 2018.

703 Kim, J. H., Sung, J. H., Chung, E.-S., Kim, S. U., Son, M., and Shiru, M. S.: Comparison of Projection in
704 Meteorological and Hydrological Droughts in the Cheongmicheon Watershed for RCP4. 5 and SSP2-
705 4.5, *Sustainability*, 13, 2066, 2021.

706 Koutsoyiannis, D.: Clausius–Clapeyron equation and saturation vapour pressure: simple theory reconciled
707 with practice, *European Journal of physics*, 33, 295, 2012.

708 Kriauciuniene, J., Jakimavicius, D., Sarauskiene, D., and Kaliatka, T.: Estimation of uncertainty sources in
709 the projections of Lithuanian river runoff, *Stochastic Environmental Research and Risk Assessment*,
710 27, 769–784, 2013.

711 Kumar, R., Musuuza, J. L., Van Loon, A. F., Teuling, A. J., Barthel, R., Ten Broek, J., Mai, J., Samaniego,
712 L., and Attinger, S.: Multiscale evaluation of the Standardized Precipitation Index as a groundwater
713 drought indicator, *Hydrology and Earth System Sciences*, 20, 1117–1131, 2016.

714 Kundzewicz, Z., Su, B., Wang, Y., Xia, J., Huang, J., and Jiang, T.: Flood risk and its reduction in China,
715 *Advances in Water Resources*, 130, 37–45, <https://doi.org/10.1016/j.advwatres.2019.05.020>, 2019.

716 Kunnath-Poovakka, A. and Eldho, T. I.: A comparative study of conceptual rainfall-runoff models GR4J,
717 AWBM and Sacramento at catchments in the upper Godavari river basin, India, *J Earth Syst Sci*, 128,
718 33, <https://doi.org/10.1007/s12040-018-1055-8>, 2019.

719 Lange, S.: Trend-preserving bias adjustment and statistical downscaling with ISIMIP3BASD (v1.0),
720 *Geoscientific Model Development*, 12, 3055–3070, <https://doi.org/10.5194/gmd-12-3055-2019>, 2019.

721 Li, D. X.: On default correlation: A copula function approach, Available at SSRN 187289,
722 <https://doi.org/10.2139/ssrn.187289>, 1999.

723 Liu, J., Zhang, Q., Singh, V. P., and Shi, P.: Contribution of multiple climatic variables and human
724 activities to streamflow changes across China, *Journal of Hydrology*, 545, 145–162,
725 <https://doi.org/10.1016/j.jhydrol.2016.12.016>, 2017.

726 Liu, Y., Hu, Z.-Z., Wu, R., and Yuan, X.: Causes and predictability of the 2021 spring southwestern China
727 severe drought, *Advances in Atmospheric Sciences*, 39, 1766–1776, 2022a.

728 Liu, Z., Deng, Z., He, G., Wang, H., Zhang, X., Lin, J., Qi, Y., and Liang, X.: Challenges and opportunities
729 for carbon neutrality in China, *Nat Rev Earth Environ*, 3, 141–155, [https://doi.org/10.1038/s43017-](https://doi.org/10.1038/s43017-021-00244-x)
730 021-00244-x, 2022b.

731 Lu, R., Xu, K., Chen, R., Chen, W., Li, F., and Lv, C.: Heat waves in summer 2022 and increasing concern
732 regarding heat waves in general, *Atmospheric and Oceanic Science Letters*, 16, 100290,
733 <https://doi.org/10.1016/j.aosl.2022.100290>, 2023.

734 Ma, N., Szilagyi, J., Zhang, Y., and Liu, W.: Complementary-Relationship-Based Modeling of Terrestrial
735 Evapotranspiration Across China During 1982–2012: Validations and Spatiotemporal Analyses,
736 *Journal of Geophysical Research: Atmospheres*, 124, 4326–4351,
737 <https://doi.org/10.1029/2018JD029850>, 2019.

738 Mallapaty, S.: China’s extreme weather challenges scientists studying it, *Nature*, 609, 888, 2022.

739 Martel, J., Demeester, K., Brissette, F., Poulin, A., and Arsenault, R.: HMETS-A simple and efficient
740 hydrology model for teaching hydrological modelling, flow forecasting and climate change impacts,
741 *International Journal of Engineering Education*, 2017.

742 Meinshausen, M., Nicholls, Z. R., Lewis, J., Gidden, M. J., Vogel, E., Freund, M., Beyerle, U., Gessner, C.,
743 Nauels, A., and Bauer, N.: The shared socio-economic pathway (SSP) greenhouse gas concentrations
744 and their extensions to 2500, *Geoscientific Model Development*, 13, 3571–3605, 2020.

745 Mokhtar, A., Jalali, M., He, H., Al-Ansari, N., Elbeltagi, A., Alsafadi, K., Abdo, H. G., Sammen, S. S.,
746 Gyasi-Agyei, Y., and Rodrigo-Comino, J.: Estimation of SPEI meteorological drought using machine
747 learning algorithms, *IEEE Access*, 9, 65503–65523, 2021.

748 Myronidis, D., Ioannou, K., Fotakis, D., and Dörflinger, G.: Streamflow and hydrological drought trend
749 analysis and forecasting in Cyprus, *Water resources management*, 32, 1759–1776, 2018.

750 Nabaei, S., Sharafati, A., Yaseen, Z. M., and Shahid, S.: Copula based assessment of meteorological
751 drought characteristics: regional investigation of Iran, *Agricultural and Forest Meteorology*, 276,
752 107611, 2019.

753 Nie, N., Zhang, W., Chen, H., and Guo, H.: A global hydrological drought index dataset based on gravity
754 recovery and climate experiment (GRACE) data, *Water Resources Management*, 32, 1275–1290,

755 2018.

756 O'Neill, B. C., Tebaldi, C., Van Vuuren, D. P., Eyring, V., Friedlingstein, P., Hurtt, G., Knutti, R.,
757 Kriegler, E., Lamarque, J.-F., and Lowe, J.: The scenario model intercomparison project
758 (ScenarioMIP) for CMIP6, *Geoscientific Model Development*, 9, 3461–3482, 2016.

759 Oudin, L., Hervieu, F., Michel, C., Perrin, C., Andréassian, V., Anctil, F., and Loumagne, C.: Which
760 potential evapotranspiration input for a lumped rainfall–runoff model?: Part 2—Towards a simple and
761 efficient potential evapotranspiration model for rainfall–runoff modelling, *Journal of Hydrology*, 303,
762 290–306, 2005.

763 Pelosi, A., Terribile, F., D'Urso, G., and Chirico, G. B.: Comparison of ERA5-Land and UERRA
764 MESCAN-SURFEX reanalysis data with spatially interpolated weather observations for the regional
765 assessment of reference evapotranspiration, *Water*, 12, 1669, 2020.

766 Perrin, C., Michel, C., and Andréassian, V.: Improvement of a parsimonious model for streamflow
767 simulation, *Journal of hydrology*, 279, 275–289, 2003.

768 Piao, S., Ciais, P., Huang, Y., Shen, Z., Peng, S., Li, J., Zhou, L., Liu, H., Ma, Y., Ding, Y., Friedlingstein,
769 P., Liu, C., Tan, K., Yu, Y., Zhang, T., and Fang, J.: The impacts of climate change on water resources
770 and agriculture in China, *Nature*, 467, 43–51, <https://doi.org/10.1038/nature09364>, 2010.

771 Pokhrel, Y., Felfelani, F., Satoh, Y., Boulange, J., Burek, P., Gädeke, A., Gerten, D., Gosling, S. N.,
772 Grillakis, M., and Gudmundsson, L.: Global terrestrial water storage and drought severity under
773 climate change, *Nature Climate Change*, 11, 226–233, 2021.

774 Porter, J. W. and McMahon, T. A.: Application of a catchment model in southeastern Australia, *Journal of*
775 *Hydrology*, 24, 121–134, 1975.

776 Pörtner, H.-O., Roberts, D. C., Poloczanska, E. S., Mintenbeck, K., Tignor, M., Alegría, A., Craig, M.,
777 Langsdorf, S., Löschke, S., and Möller, V.: IPCC, 2022: Summary for policymakers, 2022.

778 Qi, W., Chen, J., Li, L., Xu, C., Li, J., Xiang, Y., and Zhang, S.: A framework to regionalize conceptual
779 model parameters for global hydrological modeling, *Hydrology and Earth System Sciences*
780 *Discussions*, 1–28, <https://doi.org/10.5194/hess-2020-127>, 2020.

781 Rahmati, O., Falah, F., Dayal, K. S., Deo, R. C., Mohammadi, F., Biggs, T., Moghaddam, D. D., Naghibi,
782 S. A., and Bui, D. T.: Machine learning approaches for spatial modeling of agricultural droughts in the
783 south-east region of Queensland Australia, *Science of the Total Environment*, 699, 134230, 2020.

784 Ren-Jun, Z.: The Xinanjiang model applied in China, *Journal of hydrology*, 135, 371–381, 1992.

785 Schmidt, R., Schwintzer, P., Flechtner, F., Reigber, C., Güntner, A., Döll, P., Ramillien, G., Cazenave, A.,
786 Petrovic, S., and Jochmann, H.: GRACE observations of changes in continental water storage, *Global*
787 *and Planetary Change*, 50, 112–126, 2006.

788 Sherstinsky, A.: Fundamentals of recurrent neural network (RNN) and long short-term memory (LSTM)
789 network, *Physica D: Nonlinear Phenomena*, 404, 132306, 2020.

790 Shin, M.-J. and Kim, C.-S.: Component combination test to investigate improvement of the IHACRES and
791 GR4J rainfall–runoff models, *Water*, 13, 2126, 2021.

792 Shukla, S. and Wood, A. W.: Use of a standardized runoff index for characterizing hydrologic drought,
793 *Geophysical research letters*, 35, 2008.

794 Simmons, A. J., Untch, A., Jakob, C., Källberg, P., and Undén, P.: Stratospheric water vapour and tropical
795 tropopause temperatures in Ecmwf analyses and multi-year simulations, , 125, 353–386, 1999.

796 Sohn, J. A., Saha, S., and Bauhus, J.: Potential of forest thinning to mitigate drought stress: A meta-
797 analysis, *Forest Ecology and Management*, 380, 261–273,
798 <https://doi.org/10.1016/j.foreco.2016.07.046>, 2016.

799 Sönmez, A. Y. and Kale, S.: Climate change effects on annual streamflow of Filyos River (Turkey),
800 *Journal of Water and Climate Change*, 11, 420–433, <https://doi.org/10.2166/wcc.2018.060>, 2018.

801 Stewart, I. T.: Changes in snowpack and snowmelt runoff for key mountain regions, *Hydrological*
802 *Processes*, 23, 78–94, <https://doi.org/10.1002/hyp.7128>, 2009.

803 Tabari, H.: Climate change impact on flood and extreme precipitation increases with water availability,
804 *Scientific reports*, 10, 1–10, 2020.

805 Tapley, B. D., Bettadpur, S., Ries, J. C., Thompson, P. F., and Watkins, M. M.: GRACE measurements of
806 mass variability in the Earth system, *science*, 305, 503–505, 2004.

807 Tian, Y., Xu, Y.-P., and Zhang, X.-J.: Assessment of Climate Change Impacts on River High Flows
808 through Comparative Use of GR4J, HBV and Xinanjiang Models, *Water Resources Management*, 27,
809 2871–2888, 2013.

810 Tirivarombo, S., Osupile, D., and Eliasson, P.: Drought monitoring and analysis: standardised precipitation
811 evapotranspiration index (SPEI) and standardised precipitation index (SPI), *Physics and Chemistry of*
812 *the Earth, Parts A/B/C*, 106, 1–10, 2018.

813 Udall, B. and Overpeck, J.: The twenty-first century Colorado River hot drought and implications for the
814 future, *Water Resources Research*, 53, 2404–2418, 2017.

815 Vicente-Serrano, S. M., López-Moreno, J. I., Beguería, S., Lorenzo-Lacruz, J., Azorin-Molina, C., and
816 Morán-Tejeda, E.: Accurate computation of a streamflow drought index, *Journal of Hydrologic*
817 *Engineering*, 17, 318–332, 2012.

818 Wang, Z., Li, J., Lai, C., Zeng, Z., Zhong, R., Chen, X., Zhou, X., and Wang, M.: Does drought in China
819 show a significant decreasing trend from 1961 to 2009?, *Science of The Total Environment*, 579, 314–
820 324, <https://doi.org/10.1016/j.scitotenv.2016.11.098>, 2017.

821 Weinfurt, K. P.: Multivariate analysis of variance, in: *Reading and understanding multivariate statistics*,
822 American Psychological Association, Washington, DC, US, 245–276, 1995.

823 Wilhite, D. A., Svoboda, M. D., and Hayes, M. J.: Understanding the complex impacts of drought: A key to
824 enhancing drought mitigation and preparedness, *Water Resour Manage*, 21, 763–774,
825 <https://doi.org/10.1007/s11269-006-9076-5>, 2007.

826 Woolway, R. I., Kraemer, B. M., Lenters, J. D., Merchant, C. J., O’Reilly, C. M., and Sharma, S.: Global
827 lake responses to climate change, *Nat Rev Earth Environ*, 1, 388–403, [https://doi.org/10.1038/s43017-](https://doi.org/10.1038/s43017-020-0067-5)
828 020-0067-5, 2020.

829 Wu, J., Chen, X., Yao, H., and Zhang, D.: Multi-timescale assessment of propagation thresholds from
830 meteorological to hydrological drought, *Science of the Total Environment*, 765, 144232, 2021.

831 Wu, X., Guo, S., Yin, J., Yang, G., Zhong, Y., and Liu, D.: On the event-based extreme precipitation across
832 China: Time distribution patterns, trends, and return levels, *Journal of hydrology*, 562, 305–317, 2018.

833 Xiao-jun, W., Jian-yun, Z., Shahid, S., ElMahdi, A., Rui-min, H., Zhen-xin, B., and Ali, M.: Water
834 resources management strategy for adaptation to droughts in China, *Mitig Adapt Strateg Glob Change*,
835 17, 923–937, <https://doi.org/10.1007/s11027-011-9352-4>, 2012.

836 Xiujia, C., Guanghua, Y., Jian, G., Ningning, M., and Zihao, W.: Application of WNN-PSO model in
837 drought prediction at crop growth stages: A case study of spring maize in semi-arid regions of
838 northern China, *Computers and Electronics in Agriculture*, 199, 107155, 2022.

839 Xu, K., Yang, D., Yang, H., Li, Z., Qin, Y., and Shen, Y.: Spatio-temporal variation of drought in China
840 during 1961–2012: A climatic perspective, *Journal of Hydrology*, 526, 253–264, 2015.

841 Yao, F., Livneh, B., Rajagopalan, B., Wang, J., Crétaux, J.-F., Wada, Y., and Berge-Nguyen, M.: Satellites
842 reveal widespread decline in global lake water storage, *Science*, 380, 743–749,
843 <https://doi.org/10.1126/science.abo2812>, 2023.

844 Yevjevich, V. M.: Objective approach to definitions and investigations of continental hydrologic droughts,
845 An, PhD Thesis, Colorado State University. Libraries, 1967.

846 Yihdego, Y., Vaheddoost, B., and Al-Weshah, R. A.: Drought indices and indicators revisited, *Arab J*
847 *Geosci*, 12, 69, <https://doi.org/10.1007/s12517-019-4237-z>, 2019.

848 Yilmaz, M.: Accuracy assessment of temperature trends from ERA5 and ERA5-Land, *Science of The Total*
849 *Environment*, 856, 159182, <https://doi.org/10.1016/j.scitotenv.2022.159182>, 2023.

850 Yin, J., Guo, S., He, S., Guo, J., Hong, X., and Liu, Z.: A copula-based analysis of projected climate
851 changes to bivariate flood quantiles, *Journal of hydrology*, 566, 23–42, 2018.

852 Yin, J., Guo, S., Gu, L., He, S., Ba, H., Tian, J., Li, Q., and Chen, J.: Projected changes of bivariate flood
853 quantiles and estimation uncertainty based on multi-model ensembles over China, *Journal of*
854 *Hydrology*, 585, 124760, 2020.

855 Yin, J., Guo, S., Gu, L., Zeng, Z., Liu, D., Chen, J., Shen, Y., and Xu, C.-Y.: Blending multi-satellite,
856 atmospheric reanalysis and gauge precipitation products to facilitate hydrological modelling, *Journal*
857 *of Hydrology*, 593, 125878, 2021a.

858 Yin, J., Guo, S., Gentine, P., Sullivan, S. C., Gu, L., He, S., Chen, J., and Liu, P.: Does the hook structure
859 constrain future flood intensification under anthropogenic climate warming?, *Water Resources*
860 *Research*, 57, e2020WR028491, 2021b.

861 Yin, J., Guo, S., Yang, Y., Chen, J., Gu, L., Wang, J., He, S., Wu, B., and Xiong, J.: Projection of droughts
862 and their socioeconomic exposures based on terrestrial water storage anomaly over China, *Sci. China*
863 *Earth Sci.*, 65, 1772–1787, <https://doi.org/10.1007/s11430-021-9927-x>, 2022.

864 Yin, J., Gentine, P., Slater, L., Gu, L., Pokhrel, Y., Hanasaki, N., Guo, S., Xiong, L., and Schlenker, W.:

865 Future socio-ecosystem productivity threatened by compound drought–heatwave events, *Nat Sustain*,
866 6, 259–272, <https://doi.org/10.1038/s41893-022-01024-1>, 2023a.

867 Yin, J., Guo, S., Wang, J., Chen, J., Zhang, Q., Gu, L., Yang, Y., Tian, J., Xiong, L., and Zhang, Y.:
868 Thermodynamic driving mechanisms for the formation of global precipitation extremes and
869 ecohydrological effects, *Sci. China Earth Sci.*, 66, 92–110, [https://doi.org/10.1007/s11430-022-9987-](https://doi.org/10.1007/s11430-022-9987-0)
870 0, 2023b.

871 Yu, B. and Zhu, Z.: A comparative assessment of AWBM and SimHyd for forested watersheds,
872 *Hydrological sciences journal*, 60, 1200–1212, 2015.

873 Yu, Y., Si, X., Hu, C., and Zhang, J.: A Review of Recurrent Neural Networks: LSTM Cells and Network
874 Architectures, *Neural Comput*, 31, 1235–1270, 2019.

875 Zhai, P. M. and Zou, X. K.: Changes in temperature and precipitation and their impacts on drought in
876 China during 1951–2003, *Advances in Climate Change Research*, 1, 16–18, 2005.

877 Zhang, F., Deng, X., Xie, L., and Xu, N.: China’s energy-related carbon emissions projections for the
878 shared socioeconomic pathways, *Resources, Conservation and Recycling*, 168, 105456, 2021.

879 Zhang, G., Gan, T. Y., and Su, X.: Twenty-first century drought analysis across China under climate
880 change, *Climate Dynamics*, 59, 1665–1685, 2022.

881 Zhao, M., A, G., Velicogna, I., and Kimball, J. S.: Satellite Observations of Regional Drought Severity in
882 the Continental United States Using GRACE-Based Terrestrial Water Storage Changes, *Journal of*
883 *Climate*, 30, 6297–6308, <https://doi.org/10.1175/JCLI-D-16-0458.1>, 2017.

884 Zheng, J., Wang, H., and Liu, B.: Impact of the long-term precipitation and land use changes on runoff
885 variations in a humid subtropical river basin of China, *Journal of Hydrology: Regional Studies*, 42,
886 101136, 2022.

887 Zhu, Q., Luo, Y., Zhou, D., Xu, Y.-P., Wang, G., and Tian, Y.: Drought prediction using in situ and remote
888 sensing products with SVM over the Xiang River Basin, China, *Natural Hazards*, 105, 2161–2185,
889 2021.

890